DEVELOPMENT AND CHARACTERIZATION OF NOVEL ALUMINA BASED CERAMIC MATRIX COMPOSITES FOR ENERGY EFFICIENCY SLIDING APPLICATIONS

A Thesis

by

RAJESHWARI S LAKSHMI PALURI

Submitted to the Office of Graduate Studies of
Texas A&M University
in partial fulfillment of the requirements for the degree of

MASTER OF SCIENCE

August 2011

Major Subject: Mechanical Engineering

Development and Characterization of Novel Alumina Based Ceramic Matrix

Composites for Energy Efficiency Sliding Applications

DEVELOPMENT AND CHARACTERIZATION OF NOVEL ALUMINA BASED CERAMICS MATRIX COMPOSITES FOR ENERGY EFFICIENCY SLIDING APPLICATIONS

A Thesis

by

RAJESHWARI S LAKSHMI PALURI

Submitted to the Office of Graduate Studies of
Texas A&M University
in partial fulfillment of the requirements for the degree of

MASTER OF SCIENCE

Approved by:

Co-Chairs of Advisory Committee,	Hong Liang
	Sudeep Ingole
Committee Member,	Alex Fang
Head of Department,	Jerald Caton

August 2011

Major Subject: Mechanical Engineering

ABSTRACT

Development and Characterization of Novel Alumina Based Ceramic Matrix Composites for Energy Efficiency Sliding Applications. (August 2011)

Rajeshwari S Lakshmi Paluri, B.E., Osmania University, India

Co-Chairs of Advisory Committee: Dr. Hong Liang
Dr. Sudeep Ingole

Friction, wear, and lubrication have direct influence on performance, reliability, and service life of mechanical systems with moving components. The useful life of these systems and their efficiency can be improved by improving the surface properties/ performance at sliding interfaces. Further, the usage of materials for sliding systems is limited in extreme environments, such as high temperature, and space, etc., due to their limited surface properties. This thesis focuses on the development of a new class of composites with superior surface properties, i.e., low friction and high wear resistance for extreme environmental conditions. Alumina, a well understood material for its tribological performance, is a merit choice for applications where high wear resistance is required, such as pump bearings, seal rings, valve seats, piston components, gears, cutting tool inserts and artificial joints. We propose to develop a novel alumina based ceramic composite to enhance its surface and tribological properties using a powder compaction technique. The newly developed composites will be characterized by X-ray Diffraction (XRD), Fourier Transform Infrared spectroscope (FTIR), Optical

microscope, Environmental Scanning Electron Microscope (E-SEM), Goniometer and Surface profilometer. *In-situ* formation of high temperature stable phases, effect of sintering temperature, and percentage of reinforcement on phase formation will be studied. Investigation of effect of sintering temperature and percentage of reinforcement on density, porosity, and grain size will be conducted. The composites will be characterized for their tribological properties (friction and wear). The mechanisms for modified friction and wear will be proposed. The process parameters and compositions will be optimized.

XRD results confirmed the formation of $Al_{18}B_4O_{33}$, and AlB_2 and FTIR confirmed the presence of B_2O_3. Increase in sintering temperature and wt % of boron affected the porosity, grain size, and hardness of the composites. The coefficient of friction was lower for the composites compared to pure alumina ceramic. The coefficient of friction decreased with increase in sintering temperature. The wear mechanism was found to be micro-fracture using ESEM and SEM studies.

DEDICATION

This thesis is dedicated to my beloved parents, Anand & Pramod,

for their endless love and encouragement.

ACKNOWLEDGEMENTS

I would like to express my deep gratitude to my committee co-chairs, Dr. Hong Liang and Dr. Sudeep Ingole. I thank Dr. Laing for her timely advice and support. I will always be indebted to her for the opportunity she provided me. I gratefully appreciate the patience, support, guidance and wisdom of Dr. Sudeep Ingole. This thesis could not have been possible without his constant help and efforts. I thank him for instilling in me the "don't give up" attitude, which I hope to carry with me always in all my endeavors. Special thanks to my committee member Dr. Alex Fang for his interest, encouragement and willingness to help.

I also gratefully acknowledge the support provided by Dr. Vijay Panchang, Head of Department, Marine Engineering Technology, Texas A&M University at Galveston. I cannot thank him enough for providing me with financial support for the entire period of my thesis.

I express my thanks to Dr. Bhuvanesh Nattamai, Department of Chemistry for helping us with the X-ray diffraction analysis. I would also like to thank Rick Littleton, Researcher at Microscopy and Imaging Center TAMU, for helping us with ESEM. I express my gratitude to Dr. Ray Guillemette, Department of Geology and Geophysics TAMU, for helping us with the Electron Microprobe analysis.

I would also like to thank Mr. Charles Folden, Mr. James Perrigo, and Ms. Grace L. Townsend from Department of Marine Sciences TAMU, Galveston for their assistance

on chemical etching, FTIR spectroscopy, and their valuable discussions. Special thanks to Mr. Kevin Win of Marine Engineering Technology TAMU, Galveston, for his assistance during composite preparation and technical help. I would also like to thank Mr. and Mrs. Vic Penuel, from the writing center at TAMU Galveston, for their assistance. Special thanks to all the faculty and staff members at TAMU Galveston.

I especially thank my Surface Science Research group mates at Texas A&M University. Special thanks to Rodrigo Cooper, Gao Feng and David Huitink.

My life at graduate school would not have been the same without my friends. I acknowledge each and every one of them for their love and support. Especially, I thank my friends Sushma and Geetha for their constant support and the confidence that they always had in me.

Finally, I would like to thank my family for their constant support and unconditional love. I would especially like to acknowledge my mother, who is an incredible woman, who sacrificed everything in her life to make our lives easier. She made me into an independent individual and gave me the strength to fight anything and everything with courage and dignity. I am eternally grateful to my father who is also my role model. He supported me in every step I took and trusted me in every decision I made. He gave me every opportunity in life, sacrificing his needs to bring me endless joy. Thanks to my brother who is my biggest critic, also my best friend whom I always admire. Last but not the least, I express my gratitude to the love of my life, Pramod, for his patience, understanding and persistent support throughout the compilation of this thesis.

TABLE OF CONTENTS

Page

ABSTRACT iii

DEDICATION v

ACKNOWLEDGEMENTS vi

TABLE OF CONTENTS viii

LIST OF FIGURES x

LIST OF TABLES xiv

CHAPTER

I INTRODUCTION AND LITERATURE REVIEW 1

1.1. Tribology 1
1.2. Friction 2
1.3. Introduction to Ceramics 6
1.4. Properties of Ceramics 8
1.5. Toughening of Ceramics 11
1.6. Alumina and Alumina Matrix Composites 16
1.7. Tribology of Ceramics 22
1.8. Methods to Improve Friction 33

II MOTIVATION 38

III EXPERIMENTAL DETAILS 40

3.1. Materials 40
3.2. Properties 42
3.3. Composite Synthesis and Preparation 43
3.4. Physical and Mechanical Characterization 46
3.5. Surface and Tribological Characterization 55

IV CHARACTERIZATION OF ALUMINA CERAMIC COMPOSITES 59

CHAPTER Page

4.1. Physical and Mechanical Characterization 59
4.2. Surface Characterization 71
4.3. Tribological Characterization 75

V CONCLUSIONS AND FUTURE RECOMMENDATIONS 94

5.1. Physical and Mechanical Characterization 94
5.2. Surface and Tribological Characterization 95
5.3. Future Recommendations 95

REFERENCES 97

VITA 106

LIST OF FIGURES

FIGURE Page

1.1. Schematic of forces acting on a body during sliding 2

1.2. Schematic of hardness measurement..... 9

1.3. Schematic of crack bowing..... 12

1.4. Schematic of crack deflection 13

1.5. Illustration of crack bridging mechanism 14

1.6. Schematic showing adhesive and deformation forces..... 25

1.7. Schematic of adhesive wear..... 29

1.8. Schematic of abrasive wear 30

1.9. Schematic of fatigue/ delamination wear 30

1.10. Schematic of tribo-chemical wear..... 33

3.1. ESEM image of polycrystalline alumina..... 41

3.2. ESEM image of SB boron 95 powder..... 42

3.3. Across International table top laboratory pellet press..... 44

3.4. Barnstead Thermolyne 4800 muffle furnace 45

3.5. Density measurement equipment supplied by Pasco 46

3.6. Bruker-AXS D8 vario x-ray powder diffractometer..... 48

3.7. Thermo Nicolet IR300 spectrometer..... 49

3.8. Leitz MM6 large field metallographic microscope..... 50

3.9. An electro scan environmental scanning electron microscope..... 51

FIGURE Page

3.10. Cameca SX50 electron probe micro analyzer 52

3.11. LM300 vickers hardness machine 54

3.12. Mitutoyo surftest SJ 301 roughness tester 56

3.13. Home built contact angle goniometer 57

3.14 Standard CSM tribometer 58

4.1. XRD plot of composites sintered at 1200^{o}C 60

4.2. XRD spectra showing intensity change of $Al_{18}B_4O_{33}$ peak with increase in wt % of boron for composites sintered at 1200^{o}C 60

4.3. XRD plot of composites sintered at 1500^{o}C 61

4.4. XRD spectra showing intensity change of $Al_{18}B_4O_{33}$ peak with increase in wt % of boron for composites sintered at 1500^{o}C 62

4.5. Al_2O_3-B_2O_3 phase diagram 62

4.6. Aluminum rich corner of the Al-B phase diagram 63

4.7 FTIR spectra of composites sintered at 1200^{o}C 64

4.8. FTIR spectra of composites sintered at 1500^{o}C 64

4.9. Density of composites with different wt % of boron sintered at 1200^{o}C and 1500^{o}C 66

4.10 Porosity of composites with different wt % of boron sintered at 1200^{o}C and 1500^{o}C 66

4.11. Optical micrographs of (a) 1 wt % boron (b) 3 wt % composites sintered at 1200^{o}C 67

4.12. Optical micrographs of (a) 1 wt % boron (b) 3 wt % boron specimen sintered at 1500^{o}C 68

FIGURE Page

4.13. Grain size of composites with different wt % of boron sintered at 1200°C and 1500°C 69

4.14. ESEM micrographs of (a) 1 wt % boron (b) 3 wt % boron for composites sintered at 1200°C..... 69

4.15. ESEM micrographs of (a) 1 wt % boron (b) 3 wt % boron for composites sintered at 1500°C..... 70

4.16. Optical micrograph of Vickers indent 71

4.17. Surface roughness of composites with different wt% of boron for composites sintered at 1200°C..... 72

4.18. Surface roughness of composites with different wt% of boron for composites sintered at 1500°C..... 73

4.19. Contact angle of composites with different wt% of boron for composites sintered at 1200°C..... 74

4.20. Contact angle of composites with different wt% of boron for composites sintered at 1500°C..... 75

4.21. Coefficient of friction for pure alumina 76

4.22. Worn surface of steel ball used to test coefficient of friction of alumina..... 76

4.23. Average coefficient of friction of the composites..... 77

4.24. Coefficient of friction for 1 wt % boron composite sintered at 1200°C and 1500°C 79

4.25. Coefficient of friction for 2 wt % boron composite sintered at 1200°C and 1500°C 79

4.26. Coefficient of friction for 3 wt % boron composite sintered at 1200°C and 1500°C 80

4.27. Schematic of layered crystal sturcture of AlB_2..... 82

4.28. Schematic of surface porosity formed due to

FIGURE Page

decomposition of $Al_{18}B_4O_{33}$ 84

4.29. Optical micrograph of (a) wear track (b) wear scar on steel surface for 2 wt % boron composite sintered at 1200 ^oC..... 85

4.30. ESEM micrograph showing the wear track-sintered surface interface for 2 wt % boron composite sintered at 1200^oC 85

4.31. ESEM micrograph showing the wear track-sintered surface interface for 3 wt % boron composite sintered at 1200^oC 86

4.32. ESEM micrographs showing (a) composite surface (b) worn surface for 1 wt % composite sintered at 1200^oC 87

4.33. ESEM micrograph of wear track showing grain pullout and micro-cracks for composite sintered at 1200^oC 87

4.34. ESEM micrograph of wear track showing grain pullout and micro-cracks for composite sintered at 1500^oC 88

4.35. Schematic of wear scar measurement..... 89

4.36. Comparison of wear volume and coefficient of friction for composites sintered at 1200^oC..... 91

4.37. Comparison of wear volume and coefficient of friction for composites sintered at 1500^oC..... 91

4.38. SE image of wear track for 3 wt % composite sintered at 1200^oC 93

4.39. EDS spectrum of debris for 3 wt % composite sintered at 1200^oC..... 93

LIST OF TABLES

TABLE Page

1.1. Hardness values of common materials 9

1.2. Properties of different grades of alumina 18

3.1. Properties of alumina and boron 43

4.1. Properties of $Al_{18}B_4O_{33}$ and AlB_2 82

4.2. Wear volume of the steel ball at different sintering temperatures 90

4.3. Chemical composition of AISI 52100 bearing ball 92

CHAPTER I

INTRODUCTION AND LITERATURE REVIEW*

This chapter discusses the importance of low friction materials, introduces ceramics, ceramic matrix composites, tribology, friction and wear. The main focus is to understand how mechanical and tribological properties of ceramic composites are affected by the addition of reinforcement.

1.1. Tribology

Tribology has been in existence since the beginning of history. Stone Age men have created fire by rubbing surfaces of stones together. Jost first reported the word tribology in a landmark report. The term Tribology was derived from the Greek word *tribos* which means rubbing or sliding. Tribology means the study of friction, wear and lubrication [1]. Tribology was defined by British Lubrication Engineering Working group as the "*science and technology of interacting surfaces in relative motion and of related subjects and practices*". Tribology is applicable to all fields like automotives, biotechnology, biomedical, nanodevices, space engineering, etc [2].

This thesis follows the style of Tribology Letters.

1.2. Friction

Friction is defined as the resistance to relative motion between two bodies in contact. There are no ideal systems existing that do not have friction between them. When two bodies are in mutual mechanical contact and are forced to slide against each other, there will always be a friction force between them. The frictional force is always directed in the opposite direction of sliding as shown in Figure 1.1. The coefficient of friction (μ) is given by the ratio of frictional force (F) at the interface and the applied normal force (N) [3].

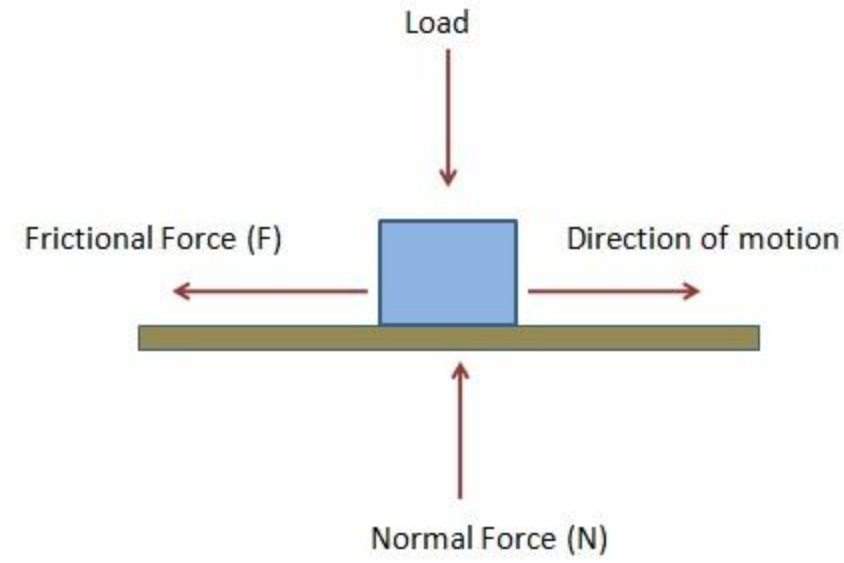

Figure.1.1. Schematic of forces acting on a body during sliding

Friction between two surfaces in contact depends on factors such as geometry, elastic properties of the material, adhesive forces, macroscopic contact points, etc. The different types of friction include sliding friction, rolling friction, static friction, and kinetic friction [4].

1.2.1. Examples of Types of Friction

Sliding friction: A block sliding down a slope surface

Rolling friction: Motor vehicle tires on road

Static friction: Car parked on a slope

Kinetic friction: Man pulling a crate on a floor

The examples explained above show that low and high friction is observed in many day to day life activities. High friction is needed in the case of motor vehicles on road to prevent them from skidding and maintaining proper traction between the road surface and the wheels. Whereas in the case of man pulling a crate on a floor, low friction is desirable in order for him to spend less energy in doing so. So, the type of friction desired depends on the application.

1.2.2. Examples of High Friction Applications

High friction is often desirable in preventing road crashes. One of the dominating reasons for the road crash is the loss of control of the vehicle. Slippery road conditions that might occur due to water on the road, spill of oil or similar substances, and/or ice formation etc. mainly causes skidding of the vehicles. Using high friction surfaces to

increase the tire traction is one of the best solutions to this problem. Thus, usage of a high friction material not only provides necessary traction for the vehicle but also leads to the energy saving as it prolongs the service life of pavements, minimize loss of life, property, and minimize maintenance issues [5].

High friction surfaces also provide better solution to high end problems without complicating designs. For example, the landing system in Mars Exploration Rover needed to drop its speed from about 17,000 mph to zero in order to settle on the surface of Mars. For that they used a mechanism which involved winding Kevlar around the brake shaft. But the rope did not stay wrapped around the shaft and started to slip down eventually due to its own weight. NASA did not give up on this idea. They came out with an idea of actually using a high friction coating with very high wear and corrosion resistance. The pads were also coated with high friction coating that keeps the equipment from moving that saved resources and expedited the mission [6].

Though high friction plays an important role in some applications, low friction is necessary to reduce energy losses and improve the performance of a system. Lubricants and surface coatings are some of the methods to reduce the friction between surfaces. Teflon is used as a coating in gears and bearings because it gives a very low coefficient of friction of ~0.1 [7]. Molybdenum disulphide coatings also give low friction values around 0.15-0.2 when tested on steel [8]. Titanium nitride is a popular coating to decrease wear and to extend the life time of drill bits [9].

1.2.3. Examples of Low Friction Applications

Maintenance of multiple rotary systems such as bearings, shafts, gearboxes, brakes, and rotors has been one of the biggest challenges in wind turbines. They operate under fluctuating loading conditions and under frequent intermittent lubrication. Condition monitoring (contamination control and oil analysis) and maintenance (lube oil, grease, filter change, etc) in wind farms are expensive. Large rolling element bearings sometimes fail catastrophically leading to prolonged downtime and repair costs. Efforts have been made to increase the minimum life cycle of turbines to 20 years by modifying the turbine architecture, using better grades of lubricants, and advanced materials for bearings. Bearings with low friction surface coatings have been used which improved the performance and increased the life cycle of turbines. Similar rolling element bearings are used in rocket engines, micro gas turbine engines, aircraft engines, turbo shafts, and turbo pumps [10, 11].

In textile industries yarn contact components require extremely low friction as well as resistance to wear and corrosion in order to prevent any surface damage to yarn. Low friction coatings have been used on several other components such as draw rolls, cooling tracks, thread guides, twist stop pins, and yarn feeders which reduce the downtime and maintenance costs. Ceramic coatings offered a very low friction and extreme wear resistance and are widely used in textile industry applications [12].

It is difficult to estimate the exact cost however, Rabinowicz estimated the annual cost of resources wasted was approximately $40 billion for engines lubrication, metal cutting

and oil drilling applications only [13, 14]. It was estimated that the annual cost of preventive measures for friction and wear losses in the United States is around $700 billion in today's economy which is approximately 6% of the gross domestic product (GDP) [15].

There is a need to develop low friction materials in order to improve the performance of mechanical systems. Efforts are being made by tribologists to develop materials with superior tribological properties. These research efforts can save approximately $150-$200 billion per year which equals 1.3% to 1.6% of the United States' gross national product (GNP) [16].

Ceramics have a higher potential in extreme environmental conditions such as high temperature, vacuum and exposure to harsh chemicals. High temperature stability, high hardness, wear resistance and chemical resistance are some of the properties which qualify them for many engineering applications compared to metals and plastics.

1.3. Introduction to Ceramics

Barsoum defined ceramic are as "*solid compounds formed by application of heat, sometimes heat and pressure, comprising of two or more elements of which one of them is a non metal or a non metallic elemental solid. The other elements may be metal(s) or nonmetallic solid(s)*". Kingery gave a simple definition to ceramics as "*non metallic inorganic materials*". For example alumina is a ceramic since it is a solid compound of metal (Aluminum) bonded to nonmetal (oxide). Magnesia, Zirconia, and Iron oxide are

some more examples. Silica is also an example of ceramic since a non metallic elemental solid combines with a non metal. Similarly Titanium carbide, Zirconium diboride, and Tungsten carbide are ceramics because metals combine with non metallic elemental solids. Boron nitride and Silicon carbide are also ceramics because it combines two non metallic elemental solids.

Ceramics can be crystalline or amorphous depending on the arrangement of atoms in the solid. Solids that exhibit long-range order are called as crystalline solids while those in which there is a lack in periodicity are called as amorphous solids. Crystalline solids exist either as single crystal or polycrystalline solids. In single crystals, the atoms are repeatedly arranged that extends throughout the entire composite without any interruption. In a polycrystalline solid, a collection of single crystals called grains are present. In ceramics the grain size ranges from 1 to 50μm. Microstructure is the combination of grains, porosity, second phases, etc. Properties of ceramics are greatly dependent on the microstructure. Ceramics are hard, brittle, high temperature resistant (refractory), corrosion and chemical resistant, electrically and thermally insulative, and have low fracture toughness. These are some of the general characteristics of ceramics. However, there are exceptions. Some ceramics are electrically and thermally conductive. Ceramics are used in cutting tools (inserts), grinding wheels, valve and ball bearings, piston components, pump bearings, spark plugs, furnace linings, switching devices, filters, turbine blades, and ceramics engines [17].

1.4. Properties of Ceramics

Following are the properties which make ceramics a merit choice for industrial applications where extreme working conditions prevail.

1.4.1. Hardness

Hardness is defined as the resistance offered by a material to plastic deformation. It depends on elastic moduli, chemical bonding, bond strength, and crystal structure of the material. High hardness is necessary for cutting tool or sliding counterface applications. Ceramics have high hardness. They are used in cutting tools, grinding wheels, turbine blades, bearings, etc.

Hardness is measured by standard techniques such as Brinell (BHN), Rockwell (HR), Knoop (HK), and Vickers (VHN) indentation. Vickers hardness test is commonly used for measuring the hardness of ceramics. An indenter is forced into the surface of a material. The applied load and the diagonals of the indent on the surface are used to measure hardness value. Figure 1.2 shows a schematic of how hardness is measured. Table.1 shows the hardness values of commonly used engineering ceramics.

Table.1.1. Hardness values of common materials [18]

Material	***Hardness (GPa)***
Diamond	76-100
Cubic Boron Nitride	45
Boron Carbide	30
Silicon Carbide	27
Alumina	25
Tungsten Carbide	19

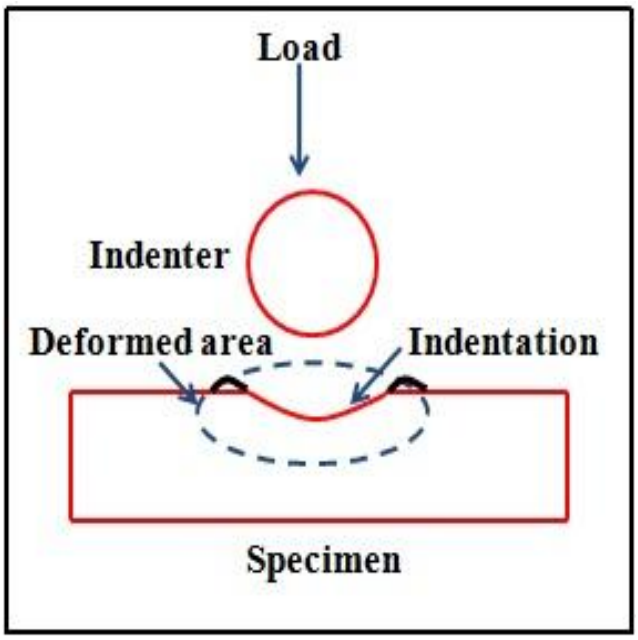

Figure 1.2. Schematic of hardness measurement

1.4.2. High Temperature Stability

High temperatures are experienced during machining, sliding of counterparts, in brake liners, and furnaces. Ceramics withstand high temperatures due to their high meting points thus making them suitable for these applications for example in cutting tools (inserts), aircraft engine gearboxes, automobiles, and industrial furnaces [19]. They are used as reinforcement in metals matrix composites to enhance their high temperature stability.

1.4.3. Corrosion Resistance/Chemical Stability

Corrosion resistance is the ability of a material to withstand the deterioration and chemical breakdown when it is exposed to harsh environments. These harsh environments include salt water, industrial chemicals, and laboratory reagents. Ceramics offer a high chemical stability and excellent corrosion resistance in highly corrosive environments. They do not react with water, acids, bases or alkalis therefore they are preferred over metals for corrosive environmental applications. They are used widely as catalysts, refractory materials artificial joints, and for chemical storage [20]. They are also used as construction materials, crockery and decorative items.

1.4.4. Fracture Toughness

The ability of a material to resist fracture/failure is called fracture toughness. It is a measure of brittleness of a material. It is an important property of a material which determines its applicability in several structural applications. Brittleness is the main

characteristic of the material with low fracture toughness. Ceramics have low fracture toughness values and hence are brittle. In order to extend and the range of applications of ceramics, improving the toughness is necessary. Toughness is increased using toughening [21].

1.5. Toughening of Ceramics

Though ceramics have good hardness, wear resistance, chemical stability and corrosion resistance, their fracture toughness is low. Understanding the toughness behavior of ceramics is important to understand their failure mechanisms. Researchers have investigated ways and methods of improving fracture toughness of ceramics. Toughness of ceramics can be bettered by controlling the microstructure [22]. Below are some of the toughening mechanisms.

1.5.1. Particle Toughening

It was found that brittle materials that contain a second phase tend to have better fracture toughness than ceramics without second phase. Increase in volume fraction of the dispersed phase increases toughness of a material. There are three ways by which toughening can occur as a result of interaction between particles that do not undergo any phase transformation and the crack front. They are crack bowing, crack deflection and crack bridging. The main aim of these mechanisms is to place obstacles in the path of the crack to impede its motion [23].

Crack bowing is a mechanism of toughening in which the reinforcement particles make the crack front non-linear and cause them to form a bowed shape between the particles due to their resistance to fracture as shown in Figure 1.3. This results a decrease in stress intensity factor (K) in the matrix along the bowed section. Crack bowing increases with increase in amount of reinforcement (by volume), reinforcement and crack interaction and the aspect ratio of the particles [24].

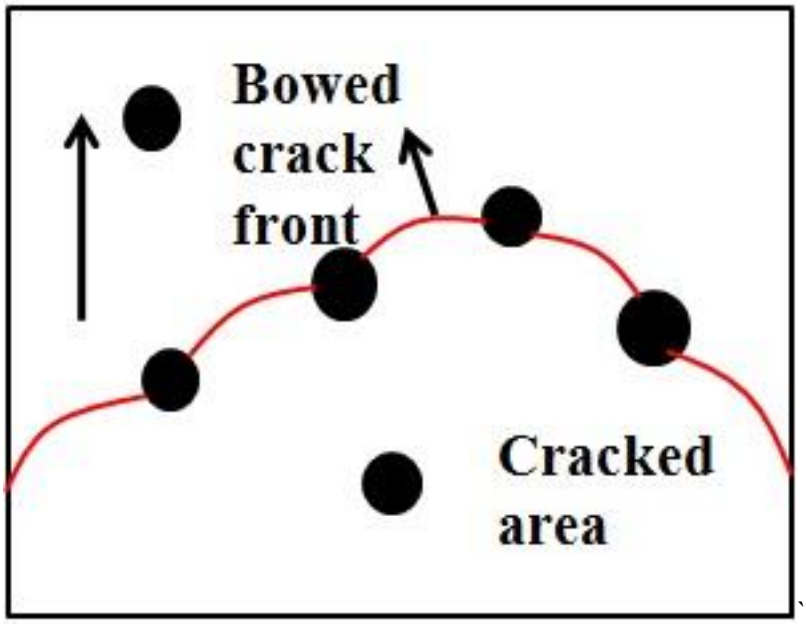

Figure 1.3. Schematic of crack bowing

In crack deflection the reinforcing particles cause the crack front to deflect around the particles thus twisting or tilting the crack from its plane of propagation as shown in

Figure 1.4. The change in crack orientation reduces the intensity of the crack extension force. The shape of the particles and volume fraction of reinforcement determine the toughening intensity. Morphologies like rod shaped grains and whiskers have been most effective for deflecting the crack [25].

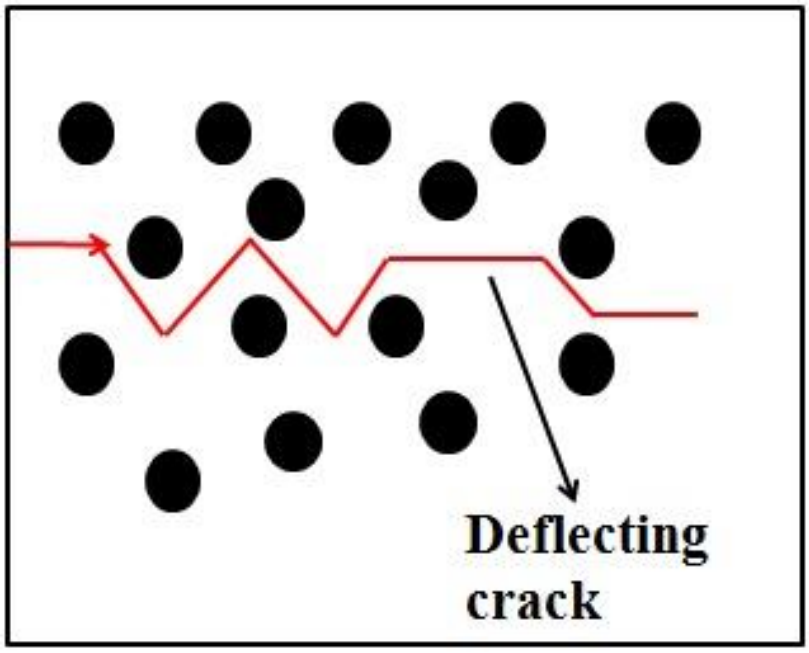

Figure 1.4. Schematic of crack deflection

Toughening is achieved by bridging of the crack surface behind the crack tip by a reinforcing phase. These bridging particles generate forces on the crack face which produce lower stress intensity at the tip (K_{tip}). This reduction slows crack propagation. The particles absorb the energy as the crack front advances. The bridging particles can

be whiskers, continuous fibers or elongated grains [17]. Figure 1.5 shows schematic of crack bridging mechanism.

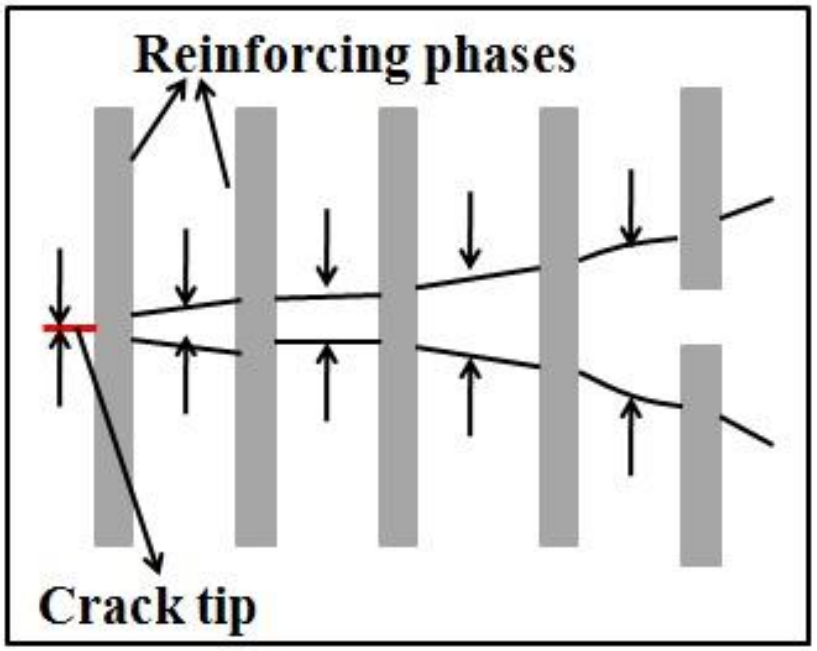

Figure 1.5. Illustration of crack bridging mechanism

1.5.2. Microcracking

Microcracks result in crack branching which leads to distribution of strain energy over a large area. This reduces the stress intensity factor at the crack tip. Crack branching increases the toughness because the stress required to propagate multiple cracks is more

than that for single crack. Zirconia toughened alumina (ZTA) is one good example for a micro-crack toughening [26].

1.5.3. *Transformation Toughening*

In ceramic composites such as ZTA, phase changes from tetragonal to monoclinic in ZTA ceramics. The volume change caused due to phase transformation in zirconia (ZrO_2) particles is used to obtain increased toughness. The second phase particles at the crack tip transform with a shear thus reducing the tensile stress concentration at the crack tip. Thus ZTA has higher toughness due to the presence of monoclinic Zirconia (ZrO_2) particles. Addition of 15% vol. ZrO_2 to a hot pressed alumina (Al_2O_3) ceramic has increased the fracture toughness from 3MPa $m^{1/2}$ [27] to 10MPa $m^{1/2}$ [28].

1.5.4. Fiber Reinforcement

Whiskers are fibrous, single crystal in structure and do not have a crystalline defect. They are prepared under controlled conditions from numerous materials like oxides, carbides, halides and organic compounds. Whisker is a single crystal which contains one dislocation running through its central axis. Whiskers have yield strength relatively closer to the maximum strength of the material [29]. The tensile strength of whisker is high (about 7GPa). Incorporating such high strength whiskers into ceramic matrices improves the flexure strength and fracture toughness. Fracture toughness of several polycrystalline matrices such as Alumina (Al_2O_3), Boron Carbide (B_4C), Silicon Nitride (Si_3N_4) and other ceramics was measured. Recent studies also show that fiber or whisker

reinforcement can also be combined with other mechanisms such as transformation toughening to achieve enhanced fracture toughness [30] .

Other factors affect the toughness of ceramics are additives, grain size, density and impurities. Tani *et al.* studied how hardness and toughness were affected by the grain in Al_2O_3 and Yttrium Oxide (Y_2O_3) ceramics. Their study showed that the fracture toughness reduced with increase in grain size. This reduction was caused due to the micro-cracks formed during thermal expansion, Y_2O_3 being cubic and Al_2O_3 being hexagonal caused local micro-stresses due to anisotropy [31].

Grain size can also result in enhanced fracture toughness of alumina based ceramics which was shows in a study by A. Muchtar *et al*. They attributed this enhancement to the shift of fracture mode from transgranular which is seen in coarse grains to the intergranular mode of fracture in submicron sized grains [32]. Another milestone in the improvement of fracture toughness of alumina ceramics was by using nano sized grains. The toughness of alumina ceramics was increased to 8 MPa $m^{1/2}$ [33].

1.6. Alumina and Alumina Matrix Composites

Alumina possesses low density, high hardness, good wear resistance and high strength which make it a good choice for structural applications. It also has low thermal conductivity, high electrical insulation, and chemical resistance [34]. It is often used in high temperature reactions as catalyst, and as a reinforcement material in metals, ceramics, and polymers matrix composites and as high temperature insulation. Alumina

is also used in cutting tools, grinding wheels and biomedical implants [35]. According to early 90's statistics, alumina ceramic have a major market as refractories, abrasives, white-wares and spark plugs, and engineering ceramics [36].

Alumina chemically known as aluminum oxide (Al_2O_3) is one of the most extensively used ceramic for engineering applications. It is abundant in nature. Alumina exists in several crystalline phases of which the most stable phase at elevated temperatures being hexagonal α phase (corundum). Alumina with α-phase is a desirable material for structural and engineering applications. Before alumina is converted to a stable phase called the α phase, there are several other intermediate meta-stable phases that are formed such as γ(Gamma), χ(Chi) , η(Eta), ε, δ(Delta) , θ(Theta)and Ќ(Kappa). Alumina is also used in catalysts, absorbents and soft abrasives. The sequence in which alumina transforms depends on material's coarseness and crystallinity, rate of heating, impurities present and the amount of water vapor in the atmosphere [37]. The properties of different grades of alumina are shown in Table 1.2.

Though, alumina has excellent mechanical and wear resistance, the fracture toughness of this material is low. This limits the applications of alumina. Therefore improving the toughness of alumina makes it more accessible to applications where increased toughness is required [38]. Toughness of alumina has increased the toughness to a range of 8- 15 $MPa.m^{1/2}$. By adding hard secondary phases such as Zirconia (ZrO_2), Titanium Carbide (TiC), Tungsten Carbide (WC), Silicon Carbide (SiC), Boron Carbide (BC_4) and

cubic-Boron Nitride (c-BN), the flexural strength and fracture toughness of alumina can be improved [39-41].

Table.1.2. Properties of different grades of alumina [42]

Property	***Mullite Ceramic 50-65% Al_2O_3 C610***	***Mullite Ceramic 65-80% Al_2O_3 C620***	***Aluminum Oxide 80-86% Al_2O_3 C780***	***Aluminum Oxide 86-95% Al_2O_3 C786***	***Aluminum Oxide 95-99% Al_2O_3 C795***	***Aluminum Oxide >99% Al_2O_3 C799***
Density (g/cc)	2.6	2.8	3.2	3.4	3.5	3.9-3.98
Hardness (GPa)	-	-	-	-	15-18	18-23
Strength (MPa)	120	150	200	250	280	300
Fracture Toughness ($MPam^{1/2}$)	-	-	-	-	4	4
Thermal Conductivity (W/mK)	2-6	6-15	10-16	14-24	16-28	19-30
Thermal Expansion ($10^{-6}K^{-1}$)	5-7	5-7	6-8	6-8	6-8	7-8

Zirconia toughened alumina (ZTA) ceramics display improved strength, hardness and fracture toughness. Zirconia is added to alumina to assist sintering. It improves the densification allowing the formation of solid solution which introduces lattice defects. Microstructures showed the presence of two distinct phases that form a solid solution. The increase in toughness is due to phase transformation and grain bridging. The transformation of phases from meta-stable tetragonal to monoclinic causes the

toughening in ZTA. The presence of zirconia grains as a second phase in the matrix enables the transformation process. A volume expansion of 4% and shear strain of 6% also occurs due to phase transformation which provides a compressive stress that eventually reduces and stops crack propagation [43, 44]. A previous work showed that the fraction of zirconia (by volume) added to alumina is directly related to the fracture resistance of the composites [45-48]. However, the hardness of the composites decreased. The lower hardness of tetragonal zirconia compared to pure alumina along with high transformability in heat treated ZTA composite caused the reduction in hardness. This transformation is inversely proportional to hardness [49, 50].

In a study by Cai *et al.* the effect of TiC on the properties of alumina was investigated. They found that both hardness and fracture toughness of the composite increased with increase in the content of TiC up to 30%. Harder TiC particles increased the overall hardness of the composite and toughness was increased due to the crack deflection, grain bridging and divergence effects produced by TiC grains. You *et al.* found that the thermal mismatch between matrix and reinforcement induced thermal stresses. These stresses blunt and arrest the micro-crack and improve the toughness of the composite. Addition of TiC reduced the grain size of alumina and improved flexural strength (σ_f), fracture toughness (K_{IC}) values which inducted an improvement in thermal shock resistance to the composite. The TiC particles also contributed to suppressing the initiation and propagation of the crack. They modified the intergranular mode of fracture in monolithic alumina to intergranular and transgranular mode of fracture in the composite. As a result, the thermal shock resistance of the ceramic improved [51, 52].

WC is a common alloy with high hardness, chemical stability and resistance to high abrasion due to which it is extensively used in machine tools and protective coatings. WC is proven to improve mechanical properties of ceramic matrix when added as a second phase. This is due to the uniform distribution of tungsten carbide particles which are irregular in shape in a fine grained dense alumina matrix. The existence of WC particles suppressed the growth of alumina grains which resulted in increase of flexural strength of the composite. When the crack meets a WC particle, the direction of crack path is tilted. Thus, introduction of a WC particle produces an intricate crack path which delays the propagation of crack by weakening the crack tip. This is responsible for toughening and strengthening the composite [53].

Mok *et al*. has investigated on the effect of addition of SiC particles to alumina matrix. Alumina-SiC composites have higher strength and hardness compared to the pure alumina matrix. But the fracture toughness remained constant. The reduction in size of the fracture initiating flaws like processing flaws compared to monolithic alumina was the reason behind the increase in strength of the composite [54-56]. In a study by Ando *et al*. alumina-SiC composites have excellent ability for crack healing. Fracture toughness of the composite was also increased and was 1.6 times higher than monolithic alumina. It was found that bridging and grain pull out effects caused by SiC whiskers led to the improvement of fracture toughness [57].

B_4C is used as reinforcement in ceramic matrix because of its high mechanical strength and Young's modulus. It was studied and postulated that by dispersing non-equiaxed

B_4C particles or whiskers in alumina matrix, the fracture toughness and flexural strength of the composite will be improved. These composites would also be lighter compared to other alumina matrix composites [58]. Liu and Ownby studied the effect of addition of boron carbide whisker to alumina matrix and the mechanisms that led to the improvement of mechanical properties of the reinforced composite. They found that the fracture toughness of the composite was considerably higher than the alumina matrix. A resistance to sudden crack propagation due to whisker pull out was evidenced. Other mechanisms that led to increase in toughness of the composites are the interactions of crack with the hard B_4C particles and also due to redistribution of stress at the crack tip when B_4C particles are encountered. The mode of interaction of the crack with the particles could be due to crack bridging, grain bridging, crack branching and crack deflection [59].

In a study by Shonhiwa *et al*. they used reaction bonded aluminum oxide (RBAO) process to produce dense alumina ceramics. RBAO is a used to produce denser alumina matrices at lower temperatures compared to conventional sintering processes. In this process, Aluminum (Al)/ Al_2O_3 powder compacts are used. They are heat treated in air so that the entire aluminum is oxidized to form Al_2O_3 to form denser monolithic composites. They also minimize the shrinkage caused during sintering. Alumina matrix composites were prepared by using c-BN as reinforcement. c-BN is the second known hardest material to diamond and it is widely used in cutting tools and abrasives industries especially for machining ferrous alloys [60, 61]. It was observed that by addition of c-BN into alumina matrix by RBAO process, the resulted composites had

higher density than the conventionally sintered composites. The densification of the composites in the reaction bonded composites was better than the conventionally sintered composites due to the fact that c-BN acts as a rigid inclusion during sintering process. The composites also showed higher hardness and fracture toughness and they also increased with increase in c-BN content. Increase in hardness is due to the higher hardness of c-BN. Crack deflection and grain bridging caused by c-BN grains improved fracture toughness. Crack deflection was mainly caused due to intrinsic stresses produced by mismatch of thermal expansion of the two phases [62].

1.7. Tribology of Ceramics

Tribology was first used in the United Kingdom in the year 1966 for describing the areas of friction, wear and lubrication. Tribology is a field of study which aims at reducing wear, increasing life of mechanical and mechatronic systems by reducing or optimizing friction. Friction and wear are unavoidable when surfaces are in contact and experience relative motion. They cannot be totally eliminated but their effects can be minimized to economically tolerable levels [63].

1.7.1. *Friction*

Friction is defined as the resistance offered by one body moving over the other. Frictional force is the force due to resistance which is tangential to the interface between sliding bodies. The relationship between frictional force and normal load is given as

$$\mu = F/N \quad (1)$$

where "μ" is the coefficient of friction, "F" is the maximum frictional force and "N" is the normal force acting on the object to be moved [1].

Friction plays an important role in our daily lives. We cannot walk without friction. Vehicles cannot ride on the roads without friction. Friction was first studied and documented by Leonardo da Vinci (1452-1519). Later, in 1699 Amontons formulated the laws of friction which are:

- Friction is proportional to the normal load
- Frictional force is independent of the apparent area of contact
- Frictional force is independent of sliding speed

Different types of friction behavior can be observed depending on material properties and the testing conditions. These variations could be due to topographical, chemical, or structural modifications of the contacting surfaces. It also includes oxidation, diffusion, melting, polishing, transformation of phases or removal of material [64].

There were several models of friction developed by various physicists. Amontons and Coulomb made important contributions to the field of tribology. They conducted experiments related to the mechanical interaction between rigid or elastically deforming asperities. Coulomb recognized that not all energy generated is available for work and non useful energy at the tribological interface is dissipated as plastic deformation or heat or formation of new surfaces through fracture [65].

Tomlinson also proposed a model for friction. He considered friction behavior in the perspective of atomic attractive and repulsive forces at the contact surface. The limitation of this model was that if there is elastic contact at atomic scale then there will be no damage on the contact surface. But material transfer is often observed on the contact surface. Therefore, tribological interactions should be on a larger scale [66].

Most current theories of sliding friction were proposed by Bowden and Tabor. This theory assumes that frictional force occurs from two sources: adhesive force and deformation force. An adhesive force required to shear the adhesive bond and a deformation force required to deform the asperities of the softer material in the path of the asperities of the harder material elastically or plastically as shown in Figure 1.6. Although in later developments of this theory they made it clear that it is convenient and illuminating to consider these two sources separately. Therefore the resultant frictional force F is the sum of adhesive force (F_{adh}) and deformation force (F_{def}) [67].

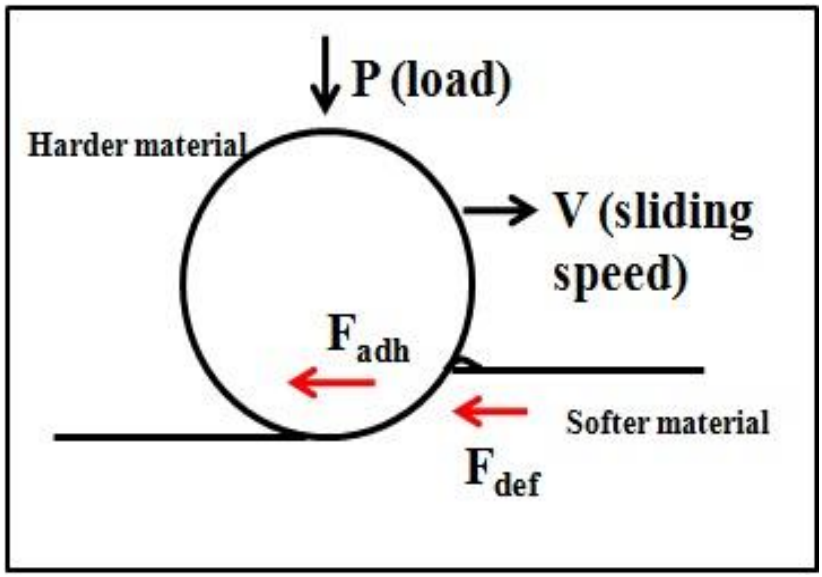

Figure 1.6. Schematic showing adhesive and deformation forces

$$F = F_{adh} + F_{def} \quad (2)$$

$$\mu = (F_{adh} + F_{def})/N \quad (3)$$

$$\mu = \mu_{adh} + \mu_{def} \quad (4)$$

In case of composites, the presence of surface films and contamination strongly affect the adhesive strength and resulting friction. Presence of oxides or absorbed films or grease prevents intimate contact between the surfaces. When a surface containing solid lubricants such as graphite dispersed in a metallic matrix comes in contact with another surface, the solid lubricant layer covers the mating surface thus reducing the adhesion friction. Thus the thin layer takes care of the adhesion part of the friction. However, the

deformation coefficient of friction is determined by the mechanical properties of the substrate [68].

Singer *et al*. studied the pressure dependence of friction of molybdenum disulfide films [69]. Bowen and Tabor also developed a theory for thin film lubrication which relates the coefficient of friction to contact pressure and expressed the coefficient of friction as

$$\mu = \tau / P \tag{5}$$

where " τ " is the shear strength of the interface and "P" is the contact pressure [67].

Bridgeman [70] proposed that at high pressures, the shear strength of the solids is dependent on pressure given by the relation

$$\tau = \tau_o + \alpha P \tag{6}$$

where " τ_o" and "α" are material properties that control friction. Then the coefficient of friction under this condition becomes

$$\mu = (\tau_o + \alpha P)/ P = (\tau_o/P) + \alpha \tag{7}$$

The mechanical property (α) and contact pressure (P) for balls and flat substrates is given by the mean Hertzian pressure. Thus by rewriting equation (5) we get,

$$\mu = \tau_o \pi (3R/4E)^{2/3} L^{-1/3} + \alpha \tag{8}$$

where “E” is the composite elastic modulus of the couple, “R” is the radius of the ball and “L” is the load. This relation applies when the loading condition is below the elastic limit. From equation (8), it can be observed that

$$\mu \propto L^{-1/3} \tag{9}$$

which shows that coefficient of friction will decrease with increase in applied load, which is not in agreement with Amontons’ and Coulomb’s explanation. This relation is valid in the case of MoS_2 films. The coefficient of friction reduced with increase in load. This behavior is also shown by diamond-like carbon (DLCs) coatings. Ball-on-flat friction tests were conducted for loads below the yield point of the substrate. The coefficient of friction reduced from 0.2 to 0.01 with an increase in contact pressure from 0.3 GPa to 1.5 GPa [71].

1.7.2. Wear Mechanisms

Wear is defined as the continuous loss of material from the sliding interfaces. Wear occurs by mechanical and/or chemical means, and by frictional heating. It is primarily a system property which depends on load, velocity, temperature, etc. Wear volume is inversely proportional to hardness given by the relation

$$V = KWL/(3H) \tag{10}$$

where “V” is the wear volume, “H” is the hardness of the wearing material, “K” is a proportionality constant called wear coefficient, “W” is the normal load, and “L” is the sliding distance [72].

Wear is usually described in terms of specific wear rate "k_w" given by the formula

$$k_w = V_w/(F.s) \quad [m^2/N] \tag{11}$$

where "V_w" is the wear volume, "F" is the load applied and "s" is the sliding distance.

Wear mechanisms are classified into adhesive wear, abrasive wear, delamination/fatigue wear, tribo-chemical wear [1].

1.7.2.1. Adhesive Wear

Adhesive wear occurs when asperities of two solids in contact adhere each other during sliding process as shown in Figure 1.7. The binding forces at the junction become stronger than that of the binding forces within the solid. The type of adhered layer formed depends on how hard the sliding materials are. In general three types of layers are formed [73]:

- Thin continuous film adhered to both contacting surfaces
- Thick continuous film adhered to both or one of the surfaces
- Thick discontinuous film adhered to both contacting surfaces

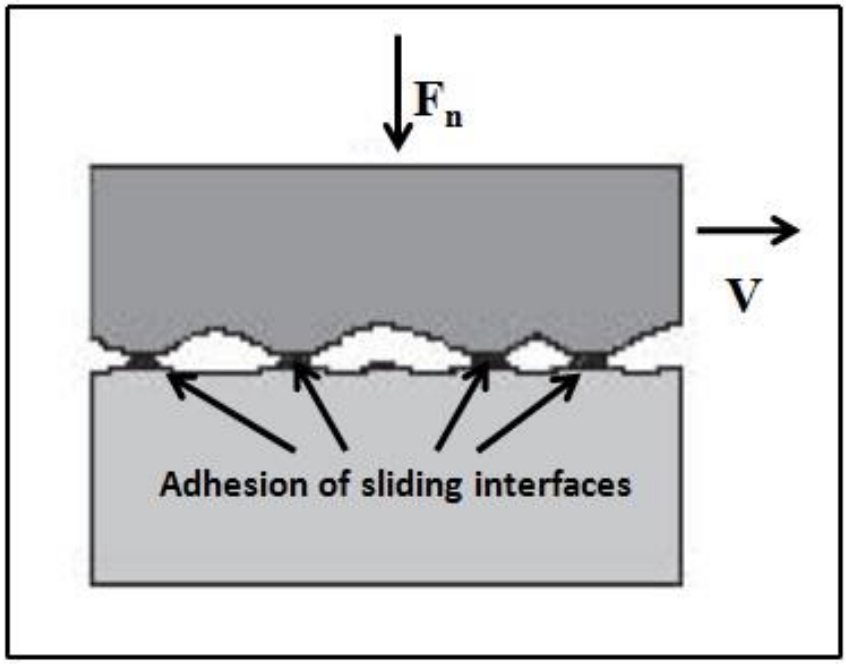

Figure 1.7. Schematic of adhesive wear

1.7.2.2. Abrasive Wear

Abrasive wear is caused by the removal or displacement of material due to the presence of hard asperities on the counterface. These hard asperities may result in grooving, ploughing or scratching depending on the properties of surfaces at interface. This mechanism is important during wear when the material is pulled out of the parent surface and is captured between the moving surfaces. If harder material is pulled out, this will act as additional abrasive material and cause wear of the softer material as shown in Figure 1.8. Hardness of a material plays a vital role in this mechanism, especially the difference in hardness between the contacting materials [74].

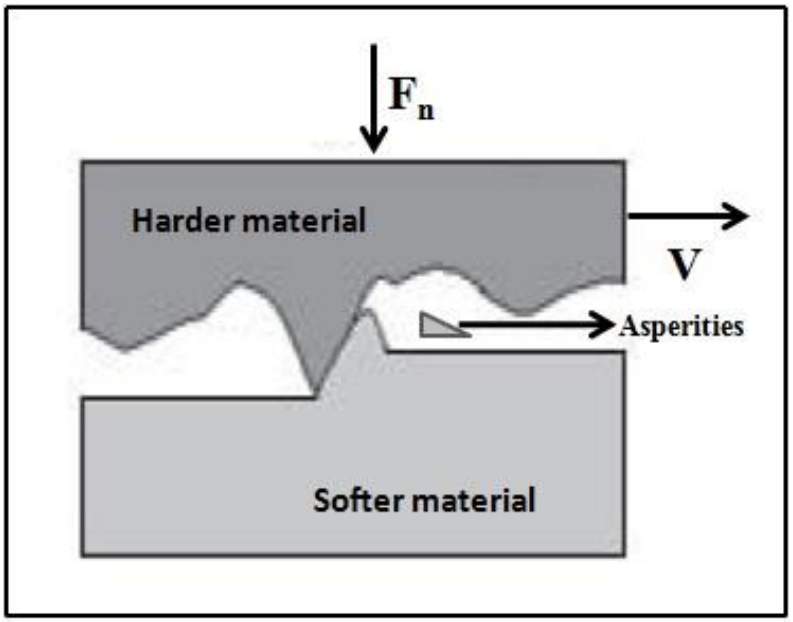

Figure 1.8. Schematic of abrasive wear

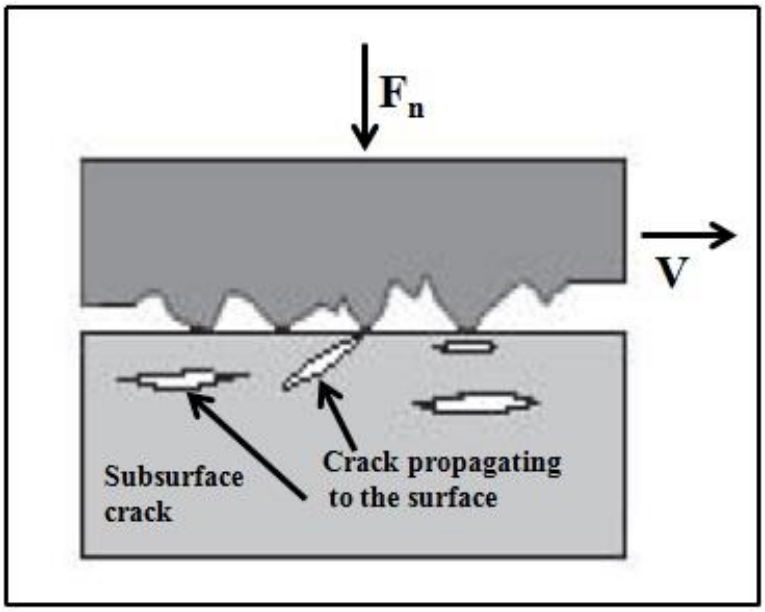

Figure 1.9. Schematic of fatigue/ delamination wear

1.7.2.3. Delamination/Fatigue Wear

Delamination is large wear of particles removed by plastic deformation of the surface layer. It is followed by nucleation of subsurface crack and crack propagation as shown in the Figure 1.9. Delamination theory is described by the following sequential steps leading to wear sheet formation which loosens from the surface.

The contact points act as an avenue to transmit the normal and tangential loads when two surfaces are in contact. Softer asperities are deformed easily due to fracture and form small wear particles where as harder asperities are removed at a slower rate. A relatively smoother surface is formed when these asperities are deformed or removed.

- Incremental plastic deformation is induced at the contact points because of the attractive force exerted by harder asperities on the surface.
- Nucleation of cracks below the surface due to increase in continuous deformation in the subsurface. The nucleation of crack does not occur very close to the surface due to existence of tri-axial compressive load right below the contact region.
- Once a crack is generated or already present, further loading and deformation causes the crack to extend and propagate. These cracks propagate parallel to the surface. The depth of the crack depends on the state of loading and properties of the material.
- Finally when the crack reaches the surface, delamination occurs from the surface as thin sheets. The location of the subsurface crack determines the

thickness of the wear sheet. Rate of crack nucleation or propagation, whichever is slower, determine the wear rate [75].

1.7.2.4.Tribo-chemical Wear

Tribo-chemical wear is mainly caused due to environmental effects divided into three types:

- Formation of layers due to absorption
- Change of surface properties due to absorption
- Formation of tribo-chemical products as shown in Figure 1.10.

The influence of environment on tribo-chemical wear is due to the moisture in the air or due to high temperatures. Tribo-oxidation wear is a common type of tribo-chemical wear. Due to friction, an increase in temperature assists the growth of an oxide layer which detaches or peels off from the surface when it reaches a critical thickness. The debris thus created either participates in the wear process or get removed from the path of sliding.

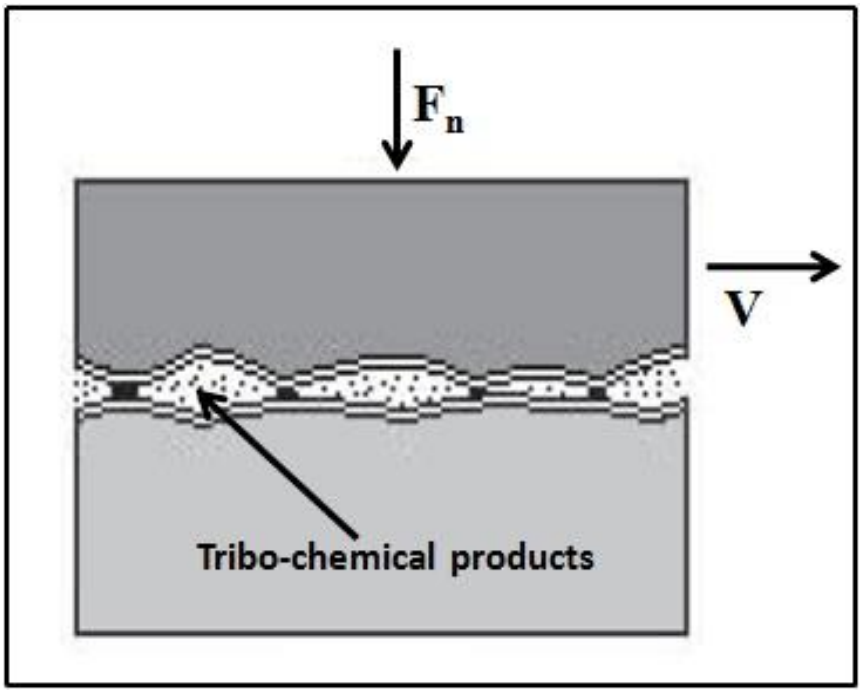

Figure 1.10. Schematic of tribo-chemical wear

The above four wear mechanisms can vary from either mild to severe wear depending on other system parameters such as load, humidity, velocity and material properties like hardness, toughness and thermal conductivity [76].

1.8. Methods to Improve Friction

Surface properties such as adhesion and friction play a vital role in the performance optimization of sliding systems ranging from micrometer to nanometer scales. The devices that include sliding systems are pump bearings, turbo-machinery parts, dental implants, prostheses joints, MEMS, and NEMS devices, etc. Surfaces with better

tribological properties can improve system efficiency [77]. Hence, there is a need to develop a new class of materials with enhanced surface properties. Surface modification treatments such as texturing, thin film layer, and coating can improve surface properties of materials.

1.8.1. Texturing

Load capacity, wear resistance, and friction coefficient were significantly improved for laser textured surfaces. Micro-dimple served either as a micro-hydrodynamic bearing or as a micro reservoir for lubricants depending on the type of lubrication. Laboratory tests showed that friction substantially decreased in textured surfaces when compared to the non-textured surfaces [78].

1.8.2. Thin Film Layer

The AFM study of self assembled monolayer (SAM) showed that hexadecane thiol (HDT) with a-CH_3 terminal exhibited lower frictional and adhesive forces. This was due to the presence of the terminal group which produced low work of adhesion. Orientation of SAMs below the critical normal load was observed. The study also reported that friction increased as humidity increased due to the higher adhesive forces in the contact zone, and it was reduced due to an enhanced water-lubricating effect [79].

1.8.3. Coatings

Wettability influences the fluid film layer and consequently both the friction and wear of the articulating surfaces in total joint arthroplasty. The wettability study of orthopedic materials such as alumina, zirconia, cobalt chrome (CoCr), and oxidized zirconium (ZrO_x) and diamond-like carbon (DLC) coating on CoCr showed that the smaller contact angles for the oxide ceramic surfaces indicate that they tend to have more wettability than metals, which may help explain their lower friction and superior adhesive wear performance [80] . Surface properties such as roughness, hydrophobic and/or hydrophilic nature of the surface influence the coefficient of friction and wear of components due to sliding [81]. The improved friction leads to better performance, energy efficiency, and sustainability. This is true in the case of high and low friction requirements.

Surface properties of a material can also be improved by adding desired friction modifier (solid lubricant). Several researchers found that incorporation of solid lubricants to metal or ceramic matrix enhanced their tribological properties. Self-lubricating ceramic matrices with soft lubricating dispersed phases have been used for various temperature tribological applications. For example, Jianxin *et al*. studied the tribological Al_2O_3/TiC ceramic composites with addition of CaF_2 as solid lubricant. Hot pressing was used to produce the composites. Addition of Calcium fluoride (CaF_2) to Al_2O_3/TiC ceramic composites gave low friction values by sliding it against cemented carbide and hardened steel counterface. The presence of CaF_2 reduced the friction values. The hexagonal

crystal structure with easy shear led to effective lubricating performance. CaF_2 which covered the worn surface acted as a solid lubricant between the material surface and the counterpart. This means that self lubrication was achieved by the presence of dispersed CaF_2 in the matrix [82].

Gangopadhyay *et al*. studied the effect of graphite on the friction and wear characteristic of alumina matrix composites. They studied the alumina-graphite containing 22% graphite. The counterpart used in their experiment was a steel ring. Although the coefficient of friction reduced from 0.5 of the alumina matrix to 0.3 of the composite, reduction in friction was not noticeable due to the absence of graphite in the transfer film. The transfer films formed on the steel counterface contained very less amount of graphite and a thick compacted layer was formed on the surface of the composite which resulted in full coverage of the graphite regions. The supply of solid lubricant is controlled by the wear of the ceramic matrix. They noticed that low wear rate of alumina-graphite composites restricted the supply of graphite to the interface. The larger wear rate of the steel counterface which produced oxides covered the graphite regions thus reducing the supply of graphite further. Their results suggest that the tribological properties of ceramic matrix composites can be improved by selecting a proper solid lubricant, matrix material and a counterface. It is important that the solid lubricant phase is not covered completely by non-lubricating wear debris. There should be enough room for the lubricating film to form on the sliding surfaces. The formation of continuous solid lubricant film is the major advantage of these composites. It allows the solid lubricant to be exposed on the surface as long as the material wears out [83].

Carrapichano *et al*. studied the effect of boron nitride (BN) on the tribological behavior of the silicon nitride (Si_3N_4) ceramics. They used hexagonal boron nitride (h-BN) platelets to enhance the tribological properties of the composite. The coefficient of friction was low compared to the pure Si_3N_4 ceramics. The decrease in friction was comparatively more when the platelets of h-BN aligned parallel to the direction of sliding. This was due to the easy shear in the direction of the crystallographic planes of h-BN particles. The coefficient of friction reduced from 0.85 to 0.65 by addition of 10% h-BN to $Si3N_4$ matrix [84].

Thus it is evident that incorporation of reinforcement into matrix material to form ceramic-matrix composites has shown a considerable improvement in mechanical and tribological properties. These multifunctional composites can be prepared to obtain tailored tribological properties to meet the industry demand.

CHAPTER II

MOTIVATION*

As discussed in Chapter I, the phenomenon of friction is an integral part of our society. It has life saving benefits such as braking systems in vehicles to prevent damage to life and property. It also has negative effects such as robbing machines of energy which otherwise could produce useful work with higher efficiency. The estimated cost of resources wasted at sliding interfaces such as piston ring/ cylinder, drill/ hole or tool/ work piece can be saved by reducing the friction. By reducing the friction at interfaces, efficiency of systems can be increased which lead to low initial and maintenance costs. It also reduces the downtime and repair costs. For example, multiple rotary systems such as bearings, gear boxes, shafts, rotors, etc with low friction surfaces increase the life time and performance of mechanical systems.

Alumina is a well understood ceramic for its tribology. It is a desirable material in many structural and engineering applications due to its hardness, high temperature stability and wear resistance. In this investigation, Alumina will be used to prepare multi-functional composites for desired properties.

---

* Reprinted with permission from Paluri, R., Ingole, S.: Surface characterization of novel alumina-based composites for energy efficient sliding systems. Journal of Materials. **63**, 77-83 (2011), Copyright [2011] by The Minerals, Metals & Materials Society.

The main objectives of this thesis are:

- Synthesis of a new class of alumina based ceramic multifunctional composites
- Characterization of phases, study of microstructure, physical, and mechanical properties of the composites
- Study of the surface properties (friction and wear) of the composites

The alumina ceramic matrix composites developed here will be useful for low friction and wear applications. They will be beneficial for the improvement of efficiency at sliding interfaces. This will lead to low maintenance costs, low downtime and improved life and performance of sliding components.

CHAPTER III

EXPERIMENTAL DETAILS*

This chapter deals with the materials, surface characterization tools and tribology, and the experimental procedure used. Alumina has always been a point of interest to ceramists and tribologists. To improve the surface, mechanical and tribological properties of alumina composites, amorphous boron was used as reinforcement. The effect of boron on the properties of alumina composites has been investigated. Alumina with boron nitride and boron carbide has been used in the field of structural and refractory ceramics and extensively investigated.

3.1. Materials

To synthesize and characterize the ceramic composite, the materials used were

3.1.1 Poly- Crystalline Alumina

Poly-crystalline 600 grit alumina powder was used as the matrix material. It is supplied by Buehler Inc. USA. The particle size of alumina used in this investigation was 14 μm. It is white/silver in appearance and is insoluble in water.

---

* Reprinted with permission from Paluri, R., Ingole, S.: Surface characterization of novel alumina-based composites for energy efficient sliding systems. Journal of Materials. **63**, 77-83 (2011), Copyright [2011] by The Minerals, Metals & Materials Society.

It does not have an odor and is lighter than air. These powders are used in lapping and polishing applications. They have been used for rough and final polishing for a long time. They are inexpensive and easily available. Poly-crystalline alumina has greater than 99% purity. Figure 3.1 is the Environmental Scanning Electron Microscope (ESEM) image of as received alumina powder.

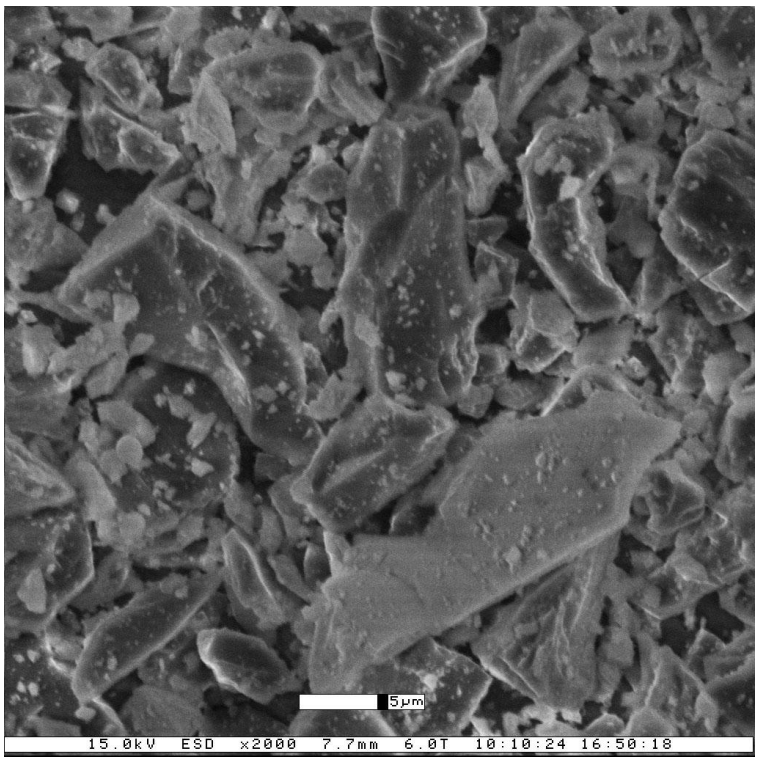

Figure 3.1. ESEM image of poly-crystalline alumina

3.1.2. Boron

Elemental amorphous boron powder (SB boron 95 fine) supplied by SB Boron Corporation, USA was used as reinforcement material. It has 95-97% Boron and other elements such as Magnesium up to 1.5%. SB boron 95 is widely used in various fields such as in aerospace, nuclear, automotive, etc. It is produced in an Argon atmosphere to prevent any contamination. Figure 3.2 is the ESEM image of as received SB boron 95 powder.

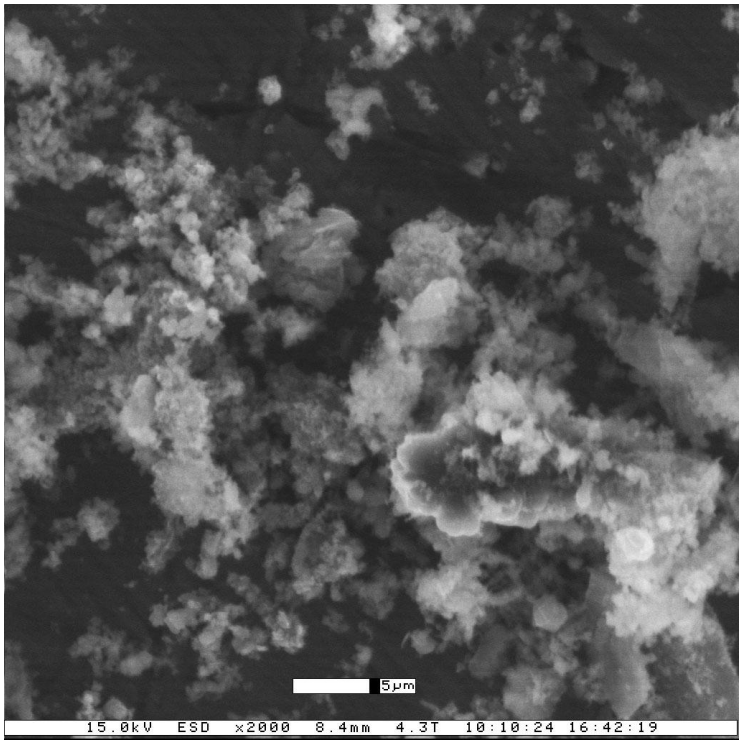

Figure 3.2. ESEM image of SB boron 95 powder

3.2. Properties

The properties of alumina and boron compounds are given in the Table 3.1.

Table 3.1. Properties of alumina and boron [85]

Material Properties	***Alumina (99.9%)***	***Boron***
Density (g/cc)	3.9	2.34
Melting point (^{o}C)	2000	2300
Young's modulus (GPa)	410	-
Hardness, (GPa)	9-12	-

3.3. Composite Synthesis and Preparation

In the development of composite material, synthesis process is a key step. There are several methods in which ceramics are synthesized. Some of them include sol-gel synthesis, gas-phase combustion, forced impregnation, etc. To synthesize the alumina composite premixing, cold compaction and sintering were used.

3.3.1 Powder Mixing and Compaction

The alumina composites were synthesized by mixing the powders uniformly with varying weight percentages (wt %) of boron to prepare green compacts. Three wt % of boron were used (i.e. 1, 2, and 3). Care was taken to avoid lumps powder particles in the mixture. Uniform mixing enables the uniform distribution of reinforced material in the

composite. A small amount of water is used as a binder. After adding water to the dry powder mixture, it is further mixed carefully.

The green powder mixture is then compacted into discs of approximately 13mm diameter and 6mm tall. A table top Laboratory Pellet Press with Built-in Hydraulic Pump and die manufactured by Across International, USA was used to prepare the green compacts. A pressure/ load of 10MPa was used for 5 minutes. The green compacts were removed carefully from the die set. Figure 3.3 shows a desktop pellet press with a built in hydraulic pump with a capacity of 15 metric tons.

Figure 3.3. Across International table top laboratory pellet press

3.3.2 Sintering

A Barnstead Thermolyne 4800 Muffle furnace as shown in Figure 3.4 was used to sinter the composites. Temperatures used to sinter the composites were 1200^{o}C and 1500^{o}C. The composites were sintered for 1 hour at a heating rate of 0.5^{0}/sec. The composites were air cooled.

Figure 3.4. Barnstead thermolyne 4800 muffle furnace

3.4. Physical and Mechanical Characterization

3.4.1 Density Measurement

Density of ceramics is determined using ASTM standard procedure C373 which is based on Archimedes's principle as shown in Figure 3.5. Archimedes' principle states that the weight of an object in a fluid is equal to its dry weight minus buoyant force. Density was calculated from weight of the composite and the volume of the fluid dispersed.

The items used in the density measurement of the composites were an over flow can, a glass beaker and pan. Kerosene was used as the working fluid. Kerosene was filled in the overflow can. A beaker was placed under the mouth of the overflow can. The composites were placed in a pan suspended with a string and then immersed in the fluid. The volume collected in the glass beaker from the overflow can was measured and the volume of the pan was subtracted. The density was determined for all the composites separately. The experiment was repeated for five times for each composite.

Figure 3.5. Density measurement equipment supplied by Pasco

3.4.2 X-Ray Diffraction (XRD)

XRD is a powerful non-destructive characterization tool for qualitative and quantitative phase analysis of crystalline materials. XRD is used to identify the crystallinity of materials. It works by the principle of Bragg's law of diffraction. A monochromatic X-ray source is used to irradiate a composite. Since this technique is sensitive to crystal structure and lattice spacing, various chemical phases and compounds can be identified. Each phase or compound has a characteristic peak defined by positions (2Theta) and intensities. A database of currently identified patterns for powder diffracted materials exists in the International Center for Diffraction Data (ICDD®).

Phase formation and identification was studied using Bruker-AXS D8 Vario X-ray powder diffractometer at Texas A&M University Chemistry department. Cu-K_α radiation as source fitted with Lynx EYE detector was used. A flat plate composite holder was used to mount the composites. The intensity (I) was recorded continuously as the composite rotates through the respective range of angles. For phase identification, measurements were recorded for a wide range of angles (2θ) ranging from 5^o to 80^o at 40Kv and 40mA. A scan speed of 0.0148 was used with an equivalent counting time of 19.2 s per step. Bruker EVA software was used for analysis. Figure 3.6 shows a picture of Bruker AXS D8 Vario X-Ray Diffractometer.

Figure 3.6. Bruker-AXS D8 vario x-ray powder diffractometer

3.4.3 Fourier Transform Infrared (FTIR) Spectroscopy

The infrared spectra (FT-IR) of the composite were recorded at room temperature. The powders of the sintered composites were prepared for the study. The composite powders were run on sodium chloride cells, on a Thermo Nicolet IR300 Spectrometer, using EZ OMNIC Version 6.0a software. Two spectra were recorded for each composite for varying sintering temperatures and compositions. Scan rate of 18 spectra per second was used. The spectrometer at Texas A&M University, Galveston as shown in Figure 3.7 was used for conducting the experiment.

Figure 3.7. Thermo Nicolet IR300 spectrometer

3.4.4 Porosity and Grain Size Measurement Using Optical Microscopy

Composites were prepared for optical microscopy by polishing from 320 grit SiC polishing paper followed by 400, 600, 800, and 1200 grit papers. Finally they were polished using a 2μm diamond paste. The composites were cleaned thoroughly with water and acetone to ensure removal of any foreign particles residing on the surface. Leitz MM6 Large Field Metallographic Microscope as shown in Figure 3.8 was used for assessment of grain size, phase formation, and porosity.

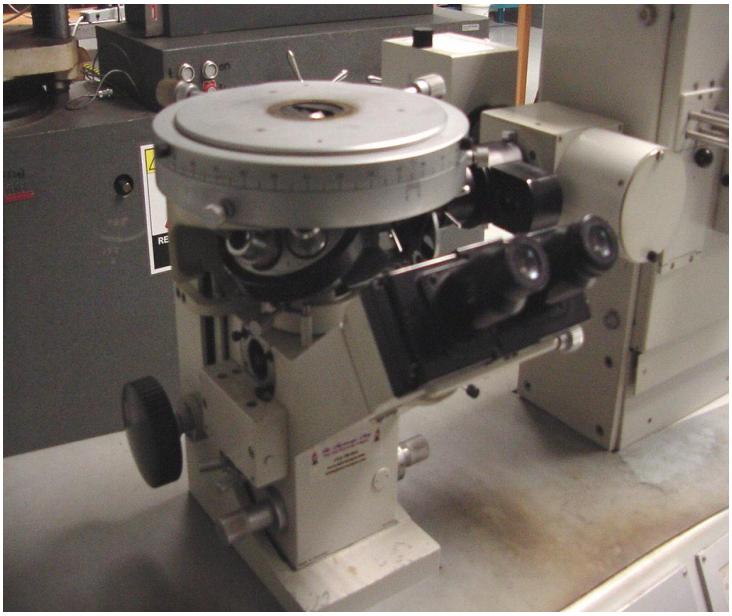

Figure 3.8. Leitz MM6 large field metallographic microscope

Mechanical properties of the ceramics depend on the micro structural characteristics such as grain size and porosity. Thus, it is essential to quantify these characteristics. The polished surfaces were etched thermo-chemically. Thermo-chemical etching involves chemical etch followed by thermal annealing at a low temperature for about 10 minutes. Chemical etching was performed with a mixture of 0.8N orthophosphoric acid and 0.5N nitric acid in the ratio of 3:1. Then they were thermally etched at $1150^{O}C$ for a duration of 10 minutes to reveal the grains [86]. Microscopic images were processed using image processing software Adobe Photoshop®. The grain size is measured as per the ASTM E112 standards [87]. ImageJ®, an image analysis software developed by National Institute of Standards and Testing (NIST) was used to measure porosity and grain size.

3.4.5 High Resolution Microscopy Study Using ESEM and SEM

An Electro Scan E3 Model ESEM as shown in Figure 3.9 was used to collect micrographs of the composite surfaces. An accelerating voltage of 15 kV was used. In Scanning Electron Microscope (SEM) high-resolution images of the composites are obtained by scanning a focused beam of electrons over the surface of a composite which is electrically conductive. A working distance of 14mm was used. The advantage of using ESEM is that it allows the non-conductive composites to be scanned without any conductive coating or preparation. The secondary electron emitted are collected and processed on the viewer monitor as a series of pixels.

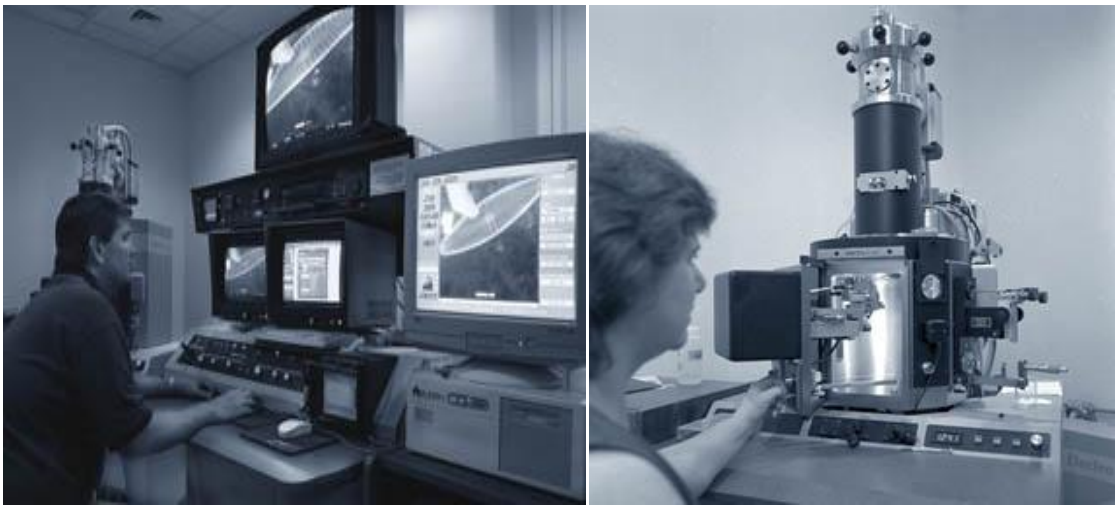

Figure 3.9. An electro scan environmental scanning electron microscope

All the polished composites were scanned using ESEM. The tribo tracks obtained from friction tests were also studied under the ESEM to understand the wear behavior of the composites. Wear tracks were scanned at different locations on the composites at different magnifications.

Figure 3.10. Cameca SX50 electron probe micro analyzer

Cameca SX 50 was used for elemental analysis of the wear track. It performs qualitative and quantitative chemical microanalysis with high accuracy. Cameca SX 50 is equipped with four wavelength dispersive X-Ray spectrometers, dispersive X-ray system and cathodoluminescence detector as shown in Figure 3.10. Its capabilities include quantitative Wavelength-Dispersive Spectrometry (WDS) analysis, qualitative and

quantitative Energy-Dispersive Spectrometry (EDS), X-ray distribution mapping, Back-Scattered Electron (BSE) imaging, Secondary Electron (SE) imaging and cathode digital imaging. Composites are polished to 0.25μm finish and coated with carbon coating of ~150 Angstroms (A^o) using a Ladd carbon evaporator to ensure conductivity. The composites are placed on a holder and placed inside the chamber for analysis. An accelerating voltage of 15 kV was used. The wear tracks were scanned to study the elements present on the composites.

3.4.6 Vickers Hardness Test

Hardness is used to measure the resistance of a material to deformation. Hardness tests are more commonly performed compared to any other mechanical test since they are simple and non-destructive. The following equation was used to calculate the hardness of the composite.

$$HVN = 1.8544\ (P/d^2)\ \text{Vickers hardness number} \quad (12)$$

$$HV = 0.0018544\ (F/d^2)\ \text{GPa} \quad (13)$$

where HVN represents the hardness value in Vickers Hardness number units and HV represents hardness in GPa. “P” is the load in newton (N) and “F” is the load in kilogram force (kgf) and “d” is the average of the diagonals of the indentation in millimeter (mm) [88].

Hardness of the composites was measured using a Leco LM300 Vickers hardness machine as shown in Figure 3.11. The load is applied using a 136^0 square based diamond

pyramid indenter. Hardness is calculated by measuring the length of diagonals on the resulting indentation surface using an optical microscope. HVN and GPa units are used to present the Vickers hardness number which is determined by dividing the load applied by the indenter by the surface area of the indenter in square millimeters(mm^2) [89].

The polished composites were tested with applied load of 1Kg for a dwell period of 13s. Six indentations were performed on each composite as recommended by the ASTM E 92 standard [90].

Figure 3.11. Leco LM300 vickers hardness machine

3.5. Surface and Tribological Characterization

3.5.1 Surface Roughness Measurement

A portable Mitutoyo Surftest SJ-301 roughness tester as shown in Figure 3.12 was used to measure the surface roughness values of the composites. The surface roughness is measured in contact mode. The roughness tester has a sharp stylus or tip attached to the detector arm. The tip traces the surface at a constant rate. The principle of working of a surface roughness tester is that the surface roughness is measured by an induction coil in the detector. The change caused in the inductive value of the coil generates an analog signal. This inductive value is proportional to the surface roughness. This analog value is converted to a digital signal which is stored and displayed on the screen of the roughness tester. The surface roughness tester can measure various parameters such as Ra, Ry, Rz, Rq, Rm, etc.

The drive/detector is attached to the height gage and the work piece/composite is placed in position. The stylus is brought in contact with the measuring surface properly and made sure that the detector is parallel to the measuring surface. The roughness values are measured and the data is processed. 'Ra' which is the arithmetic mean roughness of a surface is recorded. The displayed data is printed using an inbuilt printer. The experiment is repeated five times to ensure the accuracy. The equipment is first calibrated by using the reference composite. The radius of the tip is 10μm. A sampling length of 0.1" (2.5 mm) was used to measure the roughness. The surface roughness

values of the as sintered and polished composites for all the compositions were measured.

Figure 3.12. Mitutoyo surftest SJ 301 roughness tester

3.5.2 Contact Angle Measurement

Contact angle was measured using a home built contact angle goniometer. A video camera was attached to one of the eye pieces of a stereoscope. The composite was mounted on a holder which can be adjusted in vertical and lateral directions. Distilled water was used as a test fluid. A surgical needle and tube were used to develop fissile drops of water during experiment. A light was used in the background for better contrast of the water droplet. The assembly of the goniometer is shown in Figure 3.13. Camera was adjusted so that the entire section is devoted. An initial video image of the composite was obtained and was later processed using Windows movie maker and

Adobe Photoshop®. The contact angles on left and right of the droplet were measured using AutoCAD®. Each experiment was repeated six times and the average of the contact angles was calculated.

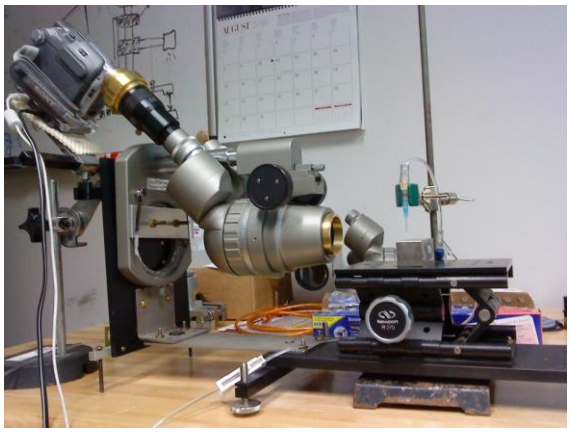

Figure 3.13. Home built contact angle goniometer

3.5.3 Friction and Wear Tests

Dry reciprocating ball-on-flat tests were performed on the composites using a CSM Tribometer as shown in Figure 3.14. This method utilizes a spherical counterpart that slides against a flat composite in a linear sliding motion. The ball was fixed rigidly in the holder and attached to the load arm. The flatness of the load arm and the composite was checked using a spirit level. All tests were conducted room temperature and at a relative humidity of 50-55%. Normal load, sliding speed, and sliding distance were monitored

throughout the test. The reciprocating tests were conducted using a track length of 6mm. A normal load of 1N was applied for a period of 30 minutes. A sliding speed of 1 cm/s was used. AISI 52100 bearing ball of 6mm diameter was used as the counterpart (sliding pair). Coefficient of friction was recorded using the data acquisition software. Average coefficient of friction was measured by considering the values at different points of time. X-Ray analysis was performed on the wear tracks. ESEM and optical microscope were used to study the worn surface morphology. EDS and SE image techniques were used to analyze the worn surfaces.

Figure 3.14. Standard CSM tribometer

CHAPTER IV

CHARACTERIZATION OF ALUMINA CERAMIC COMPOSITES*

4.1 Physical and Mechanical Characterization

4.1.1 Phase Characterization

4.1.1.1 X-Ray Diffraction (XRD)

It was observed from Figure 4.1 that Aluminum diboride (AlB_2), Boron Oxide (B_2O_3), and Aluminum Borate ($Al_{18}B_4O_{33}$) were formed at all compositions of boron when the composites were sintered at 1200^oC. With increase in wt % of boron, the intensity of $Al_{18}B_4O_{33}$ phases increased as observed from Figure 4.2. Reasons to form B_2O_3 are the sources of oxygen either from the environment as the sintering was conducted in open environment or the water used as binder.

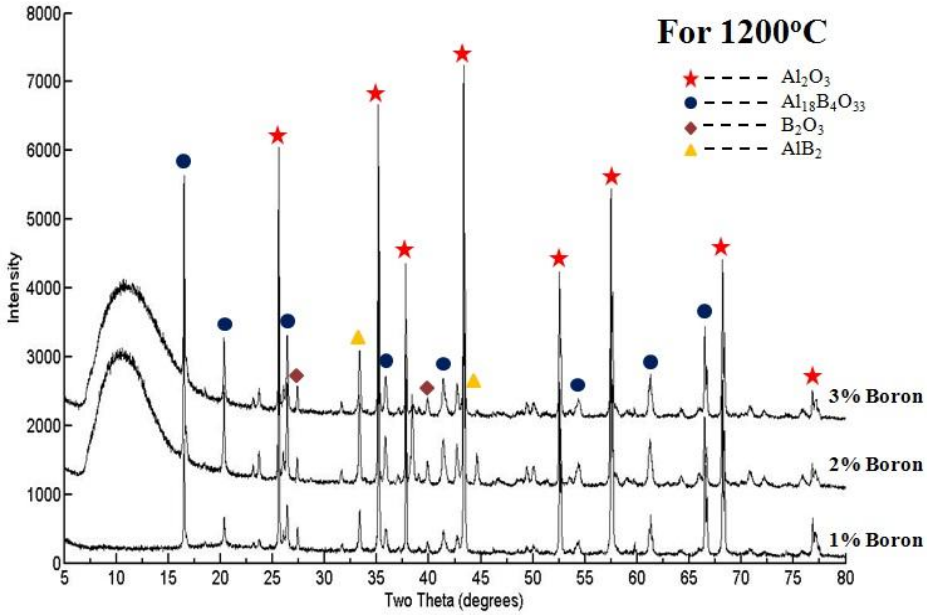

Figure 4.1. XRD plot of composites sintered at 1200°C

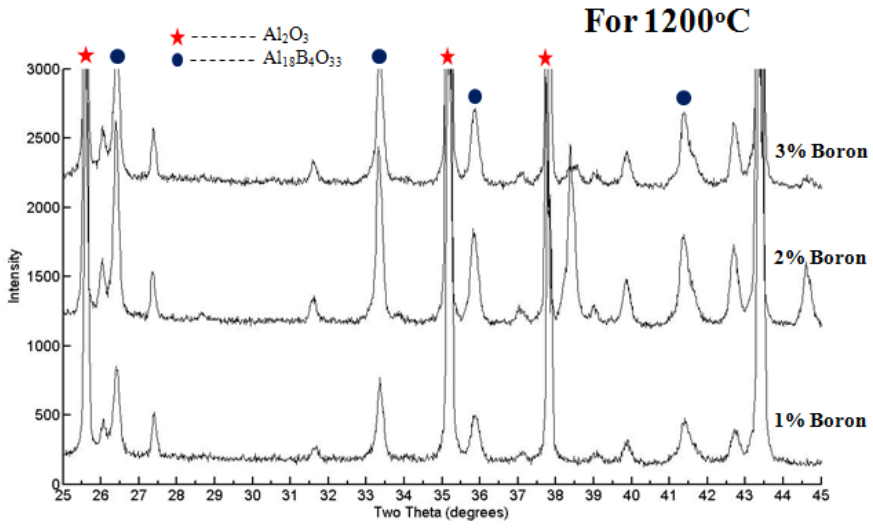

Figure 4.2. XRD spectra showing intensity change of $Al_{18}B_4O_{33}$ peak with increase in wt % of boron for composites sintered at 1200°C

For the composites sintered at 1500°C, dominating peaks of $Al_{18}B_4O_{33}$ were not observed as shown in Figure 4.3. It was observed that the formation of $Al_{18}B_4O_{33}$ reduced with increase in sintering temperature and weight percent (wt %) of boron as shown in Figure 4.4. XRD results showed the formation of AlB_2 at 1500°C. The matrix phase of Al_2O_3 was also ensured from XRD results at both sintering temperatures. $Al_{18}B_4O_{33}$ has orthorhombic crystal structure. AlB_2 and B_2O_3 have hexagonal crystal structure.

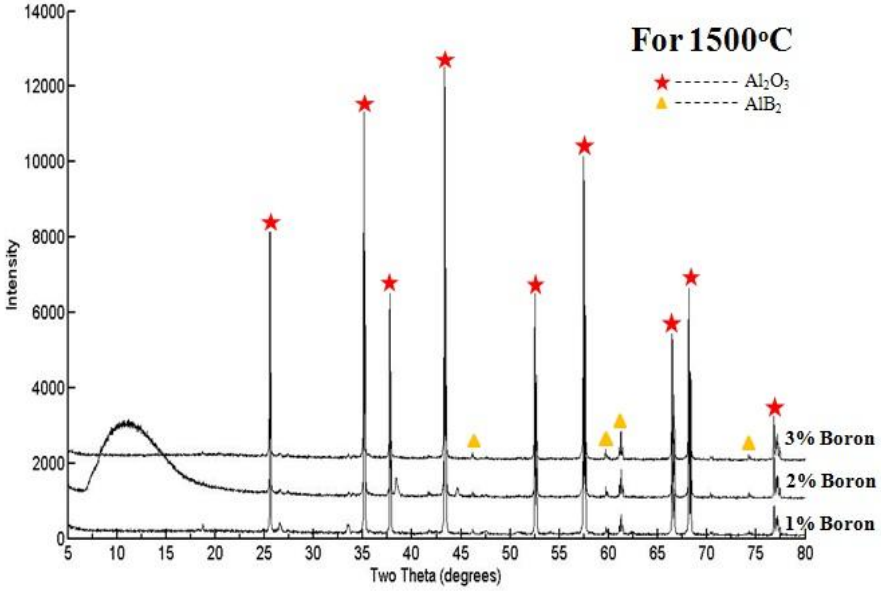

Figure 4.3. XRD plot of composites sintered at 1500°C

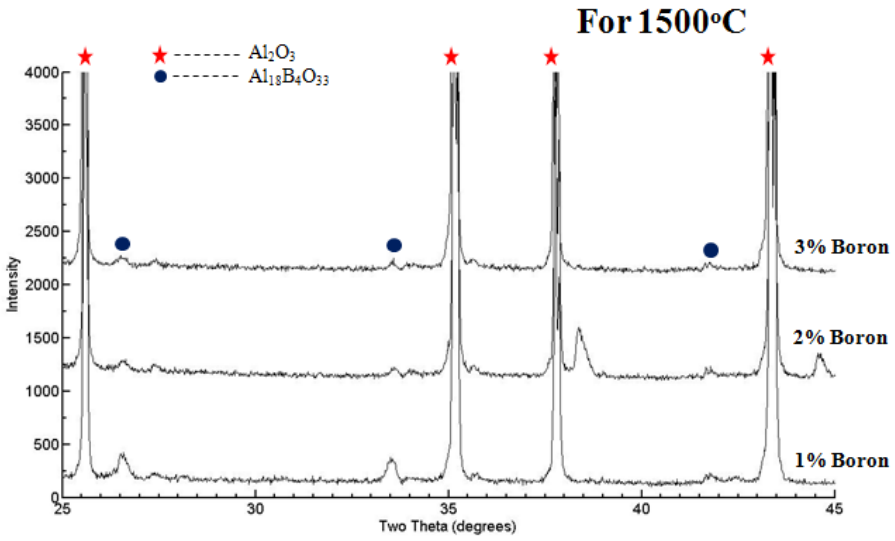

Figure 4.4. XRD spectra showing intensity change of $Al_{18}B_4O_{33}$ peak with increase in wt % of boron for composites sintered at 1500°C

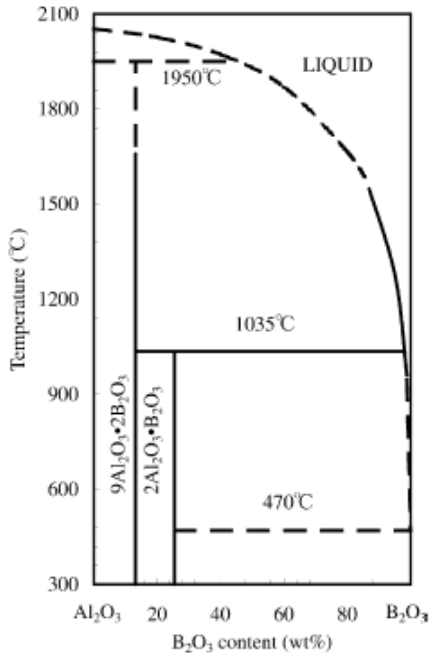

Figure 4.5. Al_2O_3-B_2O_3 phase diagram [91]

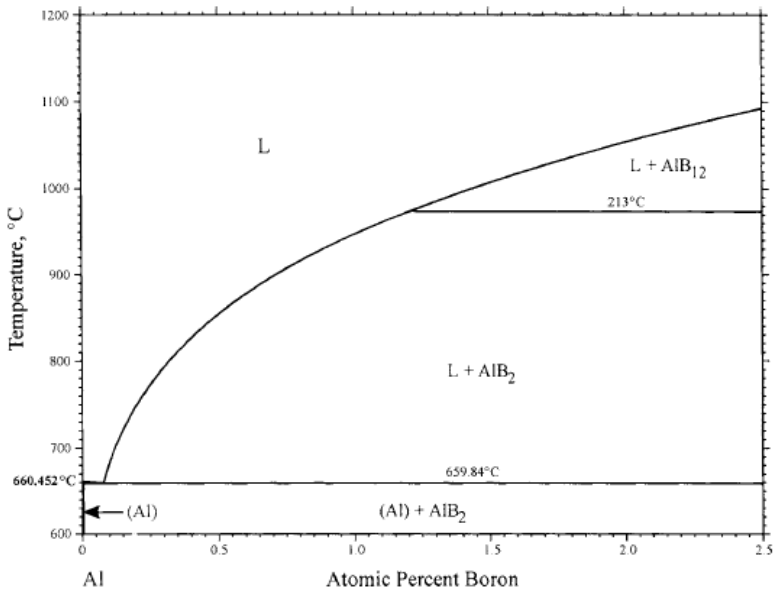

Figure 4.6. Aluminum rich corner of the Al-B phase diagram [92]

It can be observed from the phase diagrams shown in Figure 4.5 that $Al_{18}B_4O_{33}$ is an intermetallic phase forming in the presence of Al_2O_3 and B_2O_3 at low temperatures. The phase diagram of Al-B system is shown in Figure 4.6. It shows that AlB_2 forms at low temperatures and wt % of boron and is stable at high temperatures.

4.1.1.2 Fourier Transform Infrared Spectroscopy (FTIR)

In FTIR, a part of infrared (IR) rays passed through the sample is absorbed and a part of it is transmitted through the sample. The resulting spectra of absorption and transmission represent a molecule. The wavelength emitted is unique for each molecule. It is used to indentify various molecules [93]. FTIR spectra confirmed the formation of the B_2O_3 and presence of the Al_2O_3 matrix phase. The band at the wave numbers of 800cm^{-1} indicate the presence of Al_2O_3 [94]. The characteristics peaks of the B_2O_3 are present at the wave

numbers of 1458 cm^{-1}, 1195 cm^{-1} and 795 cm^{-1} [95]. The wave numbers 1414 cm^{-1} and 686 cm^{-1} correspond to the B-O-B bonds [96] as shown in Figure 4.7 and Figure 4.8.

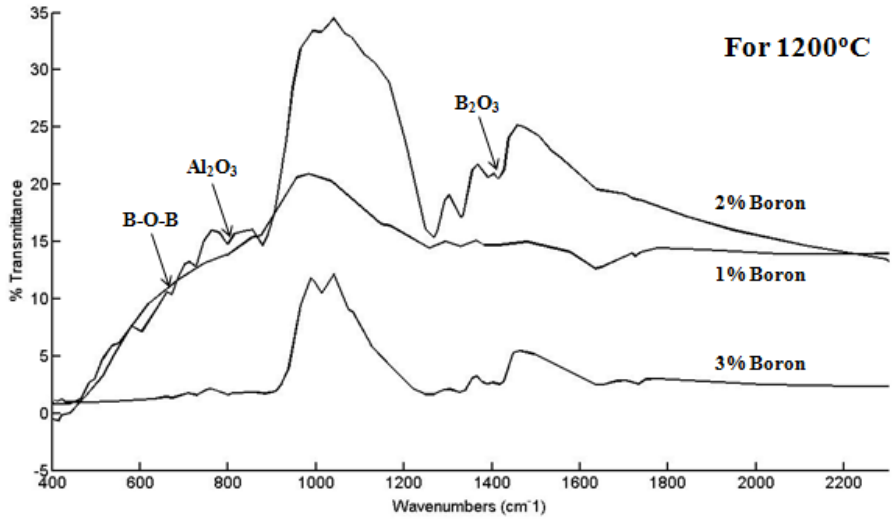

Figure 4.7. FTIR spectra of composites sintered at 1200°C

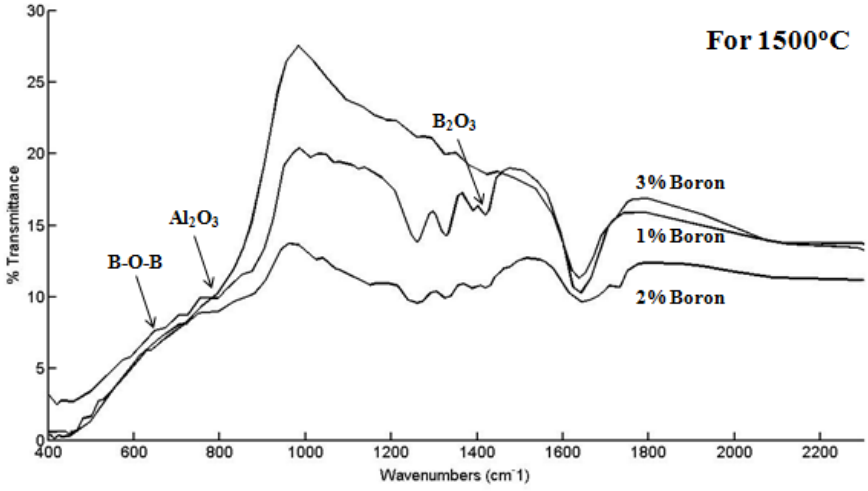

Figure 4.8. FTIR spectra of composites sintered at 1500°C

4.1.2 Effect of Sintering Temperature and Concentration of Boron on Porosity and Density

Figure 4.9 is the plot of density and wt % of boron. It was found that the density of the composite sintered at 1200^{o}C increased with increase in the wt % of boron. The increase in density with wt% of boron for composites sintered at 1200^{o}C can be attributed to the presence of $Al_{18}B_4O_{33}$. Addition of boron assisted the sintering of the alumina by providing the formation of low temperature phases such as $Al_{18}B_4O_{33}$ and AlB_2. Whereas the density of the composites decreased with increase in wt % of boron for the composites sintered at 1500^{o}C. This decrease in density could be due to the absence of aluminum borate phase in the matrix as observed from Figure 4.9. According to the XRD results, the $Al_{18}B_4O_{33}$ phase was not stable at higher temperature.

At the same time, the porosity of these composites decreased with increase in wt % of boron for composites sintered at 1200^{o}C. The porosity of the composites sintered at 1500^{o}C increased with increase in wt% of boron as shown in Figure 4.10. The porosity results are in agreement with densities of the composites.

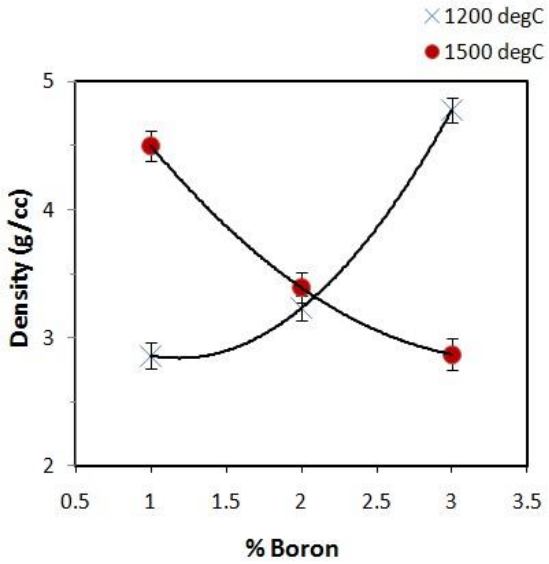

Figure 4.9. Density of composites with different wt % of boron sintered at 1200^{o}C and 1500^{o}C

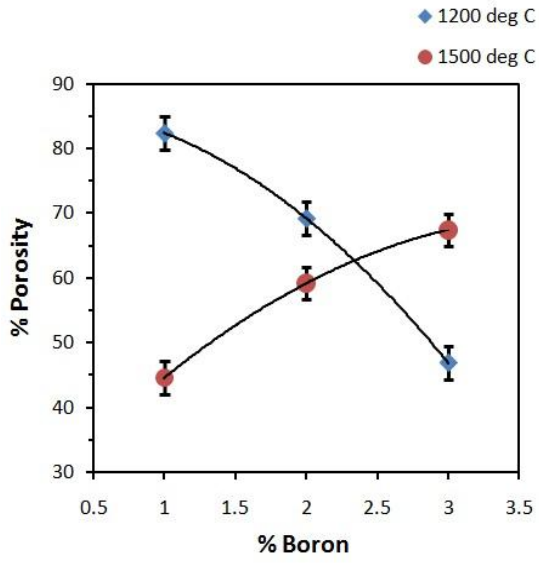

Figure 4.10. Porosity of composites with different wt % of boron sintered at 1200^{o}C and 1500^{o}C

Figures 4.11 and 4.12 show the effect of sintering temperature on surface porosity. It is evident from these figures that the surface porosity increased with wt % of boron and sintering temperature. Porosity of 3 wt % boron composite sintered at 1200^{o}C was less than the porosity of 1 wt % boron composite.

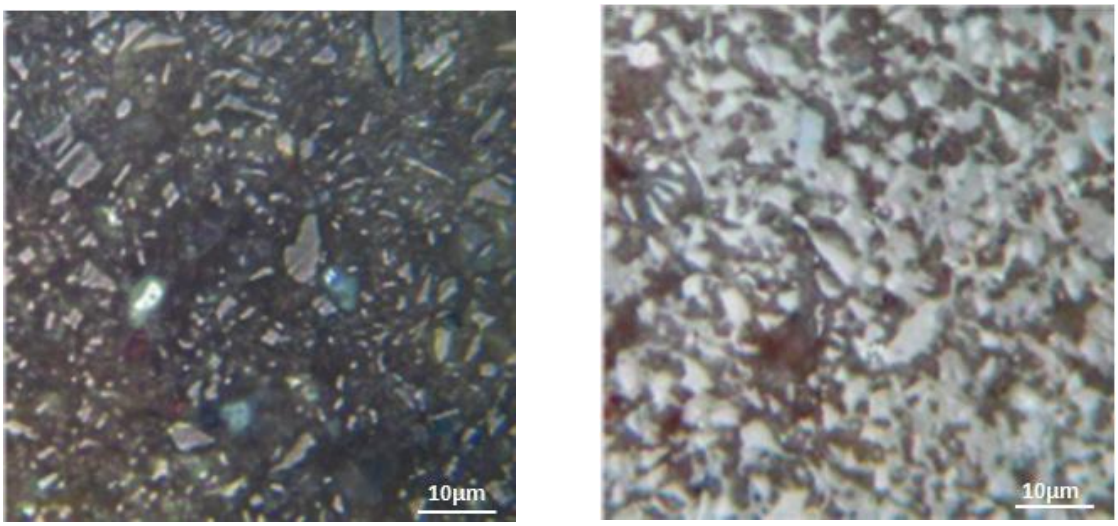

(a) (b)

Figure 4.11. Optical micrographs of (a) 1 wt % boron (b) 3 wt % boron composites sintered at 1200^{o}C

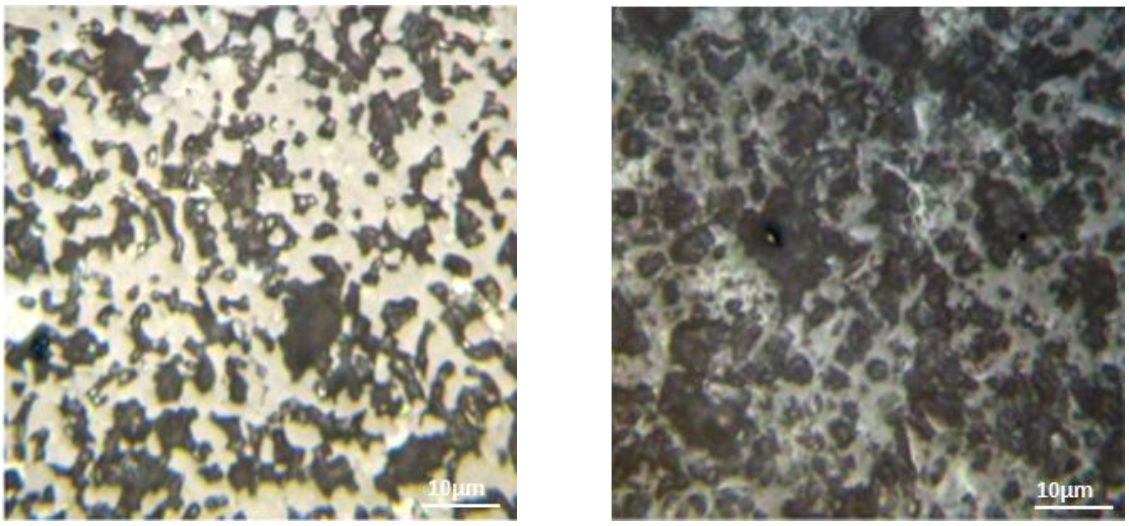

(a) (b)

Figure 4.12. Optical micrographs of (a) 1 wt % boron (b) 3 wt % boron composites sintered at 1500°C

4.1.3 Effect of Sintering Temperature and Concentration of Boron on Grain Size

Figure 4.13 illustrates the effect of wt % of boron on the grain size for composite sintered at 1200°C and 1500°C. It was observed that the grains size of composites decreased with increase in wt % of boron for both the sintering temperatures. Diffusion of grain boundaries is evident from Figure 4.14 and Figure 4.15 when wt % of boron increased for the composites sintered at 1200°C and 1500°C. The segregation of secondary phases at the grain boundaries might have restricted the grain growth. This might have caused a reduction in grain size with increase in sintering temperature and wt % of boron. This trend is more prominent for the composite sintered at 1500°C.

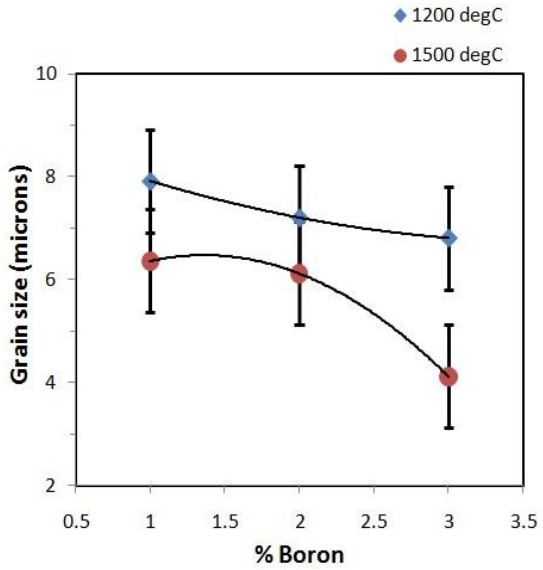

Figure 4.13. Grain size of composites with different wt % of boron sintered at 1200^{o}C and 1500^{o}C

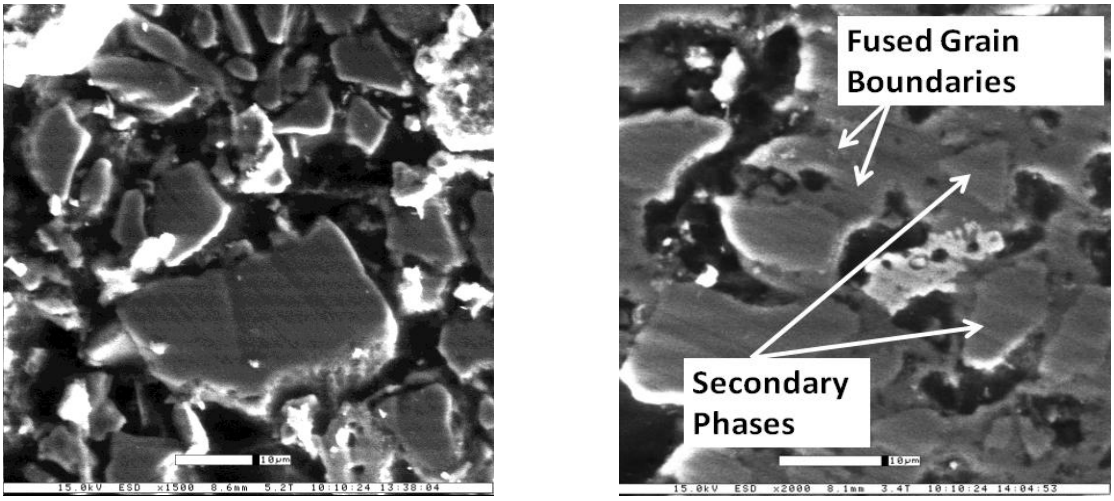

(a) (b)

Figure 4.14. ESEM micrographs of (a) 1 wt % boron (b) 3 wt % boron for composites sintered at 1200^{o}C

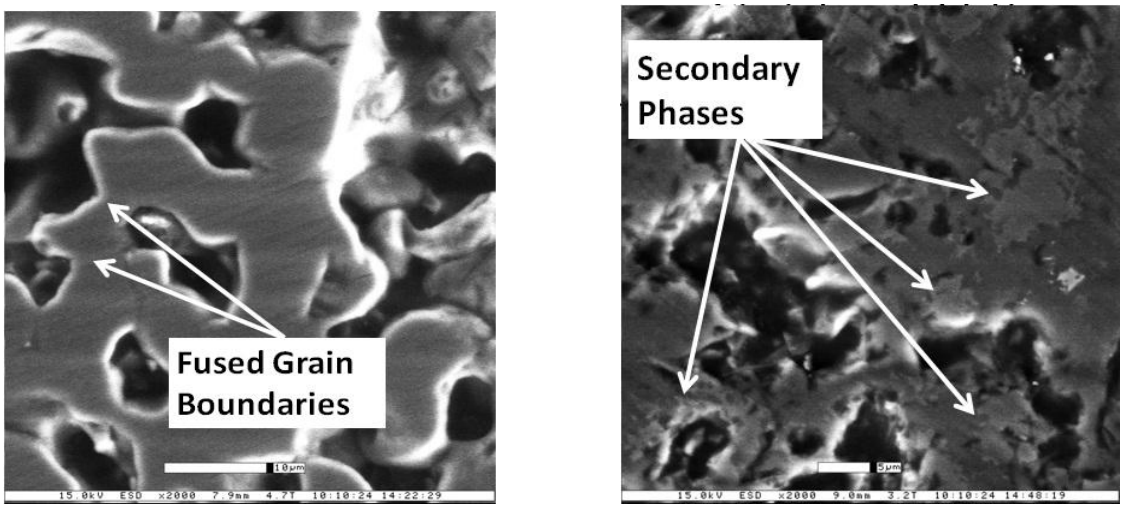

(a) (b)

Figure 4.15. ESEM micrographs (a) 1 wt % boron (b) 3 wt % boron for composites sintered at 1500^{o}C

4.1.4 Effect of Sintering Temperature and Concentration of Boron on Hardness

It was found that the hardness of the composite increased with increase in wt % of boron for the composites sintered at 1200^{o}C. The formation of hard $Al_{18}B_4O_{33}$ (secondary phases) increased the hardness for the composites sintered at 1200^{o}C. These secondary phases were uniformly distributed in the cross-section. The hardness of the composites sintered at 1500^{o}C decreased with increase in wt % of boron. The decrease in hardness might be due to the presence of absence of $Al_{18}B_4O_{33}$ and higher surface porosity. Figure 4.16 is the optical micrograph of Vickers indent.

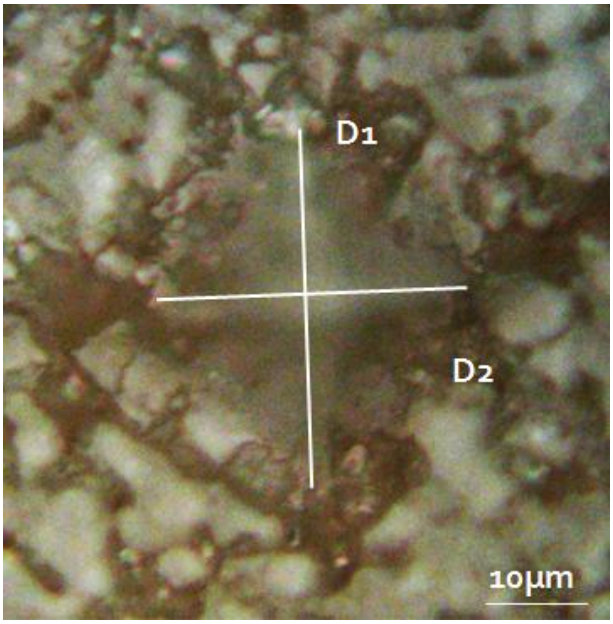

Figure 4.16. Optical micrograph of Vickers indent

4.2 Surface Characterization

4.2.1 Effect of Sintering Temperature and Concentration of Boron on Surface Roughness

Figure 4.17 and Figure 4.18 show the effect of sintering temperature and wt % boron on surface roughness. It is observed that the surface roughness of the as sintered composites at 1200^{o}C decreased with increase in wt% of boron. For the as sintered composites at 1500^{o}C, the surface roughness increased with an increase in wt% of boron. The increase in surface roughness might be due to the increase in porosity of composites sintered at 1500^{o}C. The decomposition of orthorhombic $Al_{18}B_4O_{33}$ phase

changed the texture of the sintered composites. But with increase in sintering temperature and wt% of boron, the surface roughness of the composites decreased after polishing. This change in surface texture might as well change the friction and wear behavior of the composites.

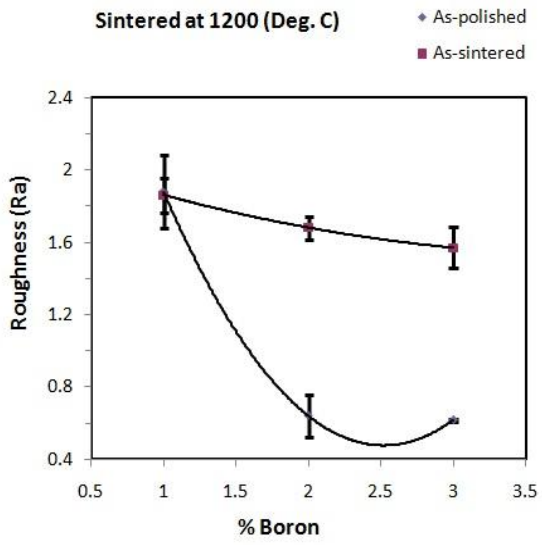

Figure 4.17. Surface roughness of composites with different wt % of boron for composites sintered at 1200^{o}C

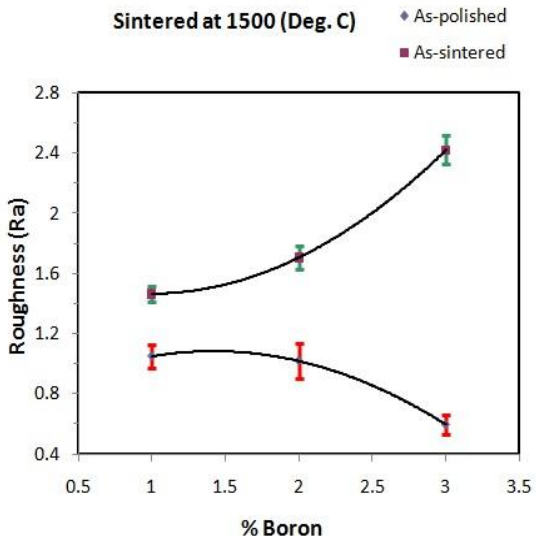

Figure 4.18. Surface roughness of composites with different wt % of boron for composites sintered at 1500^{o}C

4.2.2 Effect of Sintering Temperature and Concentration of Boron on Contact Angle

Figure 4.19 and Figure 4.20 show the effect of sintering temperature and wt% of boron on contact angle. It can be observed that the contact angle increased with increase in wt% of boron for as sintered composites at 1200^{o}C. For as sintered composites at 1500^{o}C, the contact angle decreased with increase in wt% of boron. The decrease in contact angle with increase in wt% of boron for the composites sintered at 1500^{o}C could be due to the presence of higher surface porosity. The contact angle values for as sintered composites at 1200^{o}C and 1500^{o}C were less than 90° which shows that they were hydrophilic. For the as polished composites at 1200^{o}C and 1500^{o}C, the contact

angles were more than 90° which shows that after polishing, the surfaces were converted to hydrophobic.

A surface is hydrophobic if it does not tend to be wetted by water. The contact angle on hydrophobic surfaces is ~120°. A surface is hydrophilic if it tends to be wetted by water. The contact angle on hydrophilic surface is <90° [97]. The average contact angle for as polished composites at 1200°C and 1500°C was approximately 115° and 105° respectively.

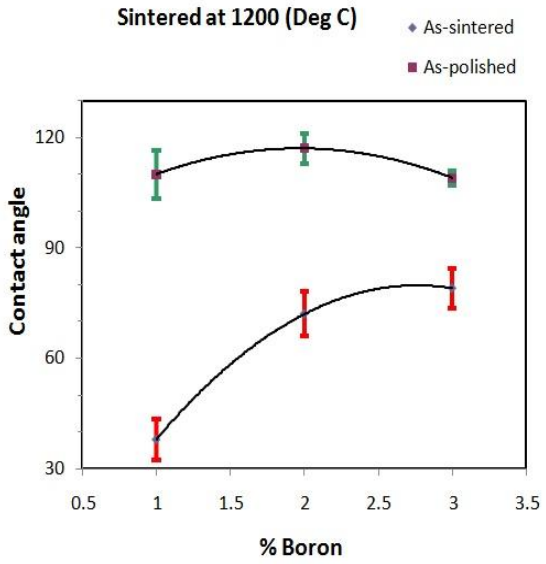

Figure 4.19. Contact angle of composites with different wt % of boron for composites sintered at 1200°C

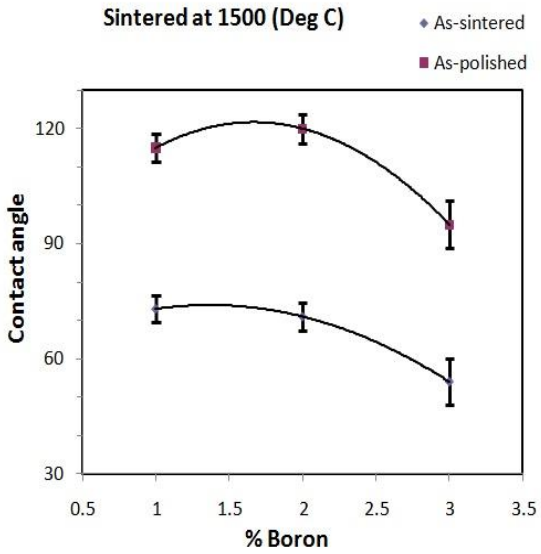

Figure 4.20. Contact angle of composites with different wt % of boron for composites sintered at 1500^{o}C

4.3 Tribological Characterization

4.3.1 Friction Behavior

Figure 4.21 shows the graph of coefficient of friction for pure alumina. The initial coefficient of friction was a higher value of 0.45. This value gradually increased with time. It was 0.52 at the end of the test period. This value is lesser than the literature value which is ~0.9-1 [98]. Gradual increase in coefficient of friction for pure alumina might be due to increase in contact area between steel ball and alumina surface as the test continued. The worn surface on the steel ball is elliptical as the wear track deepened with time as seen in Figure 4.22.

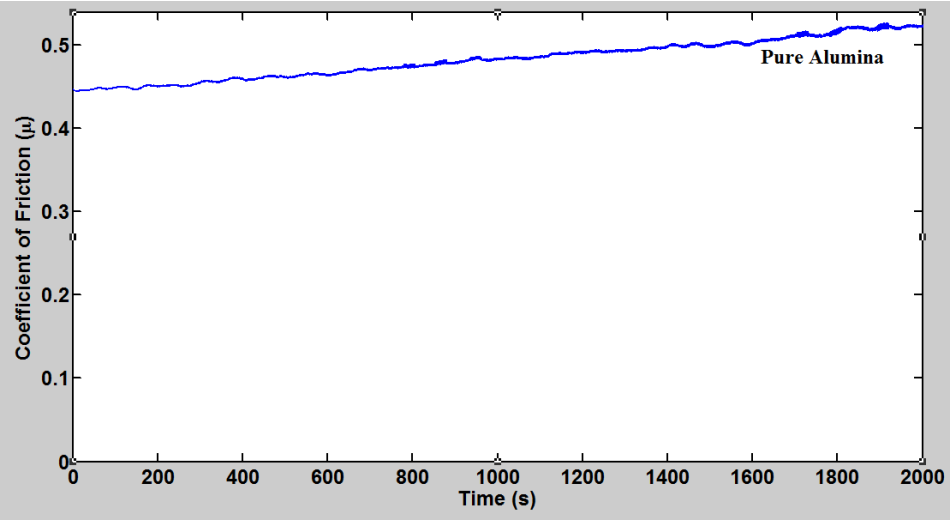

Figure 4.21. Coefficient of friction for pure alumina

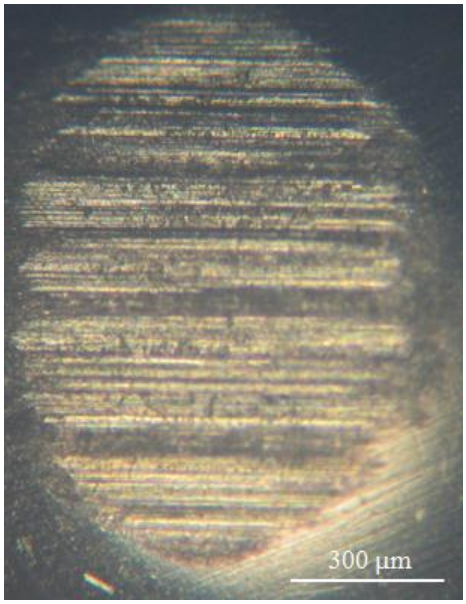

Figure 4.22. Worn surface of steel ball used to test coefficient of friction of alumina

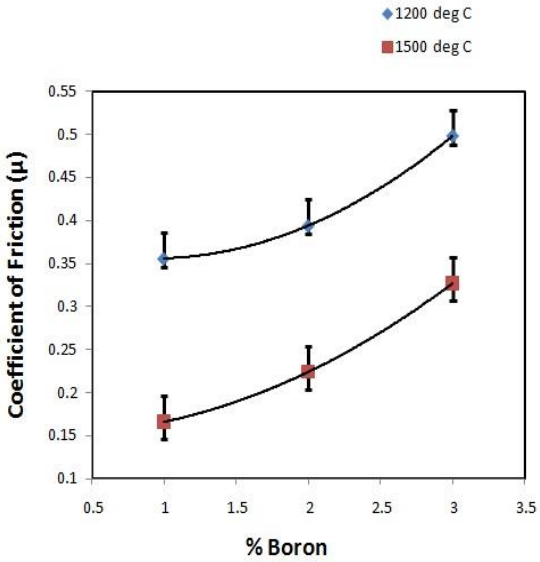

Figure 4.23. Average coefficient of friction of the composites

Figure 4.23 shows the average coefficient of friction for all the composites. Composites sintered at 1500^{o}C have lower friction values compared to those sintered at 1200^{o}C. The coefficient of friction of the composites (Figure 4.23) was comparatively lesser than alumina (Figure 4.21). It was found that the coefficient of friction increased with increase in wt % of boron for composites sintered at 1200^{o}C and 1500^{o}C. The lowest coefficient of friction for composites sintered at 1200^{o}C was 0.37 (± 0.03) for 1 wt % boron composite. The highest value was for 3 wt % boron composite which was 0.54 (± 0.04). For the composites sintered at 1500^{o}C the lowest was 0.19 (± 0.01) for 1 wt % boron composite. Highest value was observed for 3 wt % boron composite which was 0.32 (± 0.01).

Figure 4.24 shows the comparison of coefficient of friction for 1 wt % boron composites sintered at 1200^{o}C and 1500^{o}C. At the beginning of the test, the coefficient of friction was lower for the composites sintered at 1200^{o}C (0.25). It gradually increased and stabilized at an average value of 0.37. For the composite sintered at 1500^{o}C, the coefficient of friction initially started at a higher value of 0.32. It gradually decreased with time and stabilized at a value of 0.18 by the end of the test period.

The comparison of coefficient of friction for 2 wt % boron composite sintered at 1200^{o}C and 1500^{o}C in Figure 4.25. The friction behavior is similar to the 1 wt % boron composite as explained above. The coefficient of friction was lower (0.22) for the composites sintered at 1200^{o}C at the start of the test. It gradually increased and stabilized at an average value of 0.39. For the composite sintered at 1500^{o}C, the coefficient of friction initially started at a higher value of 0.3. It gradually decreased with time and stabilized at a value of 0.21 by the end of the test.

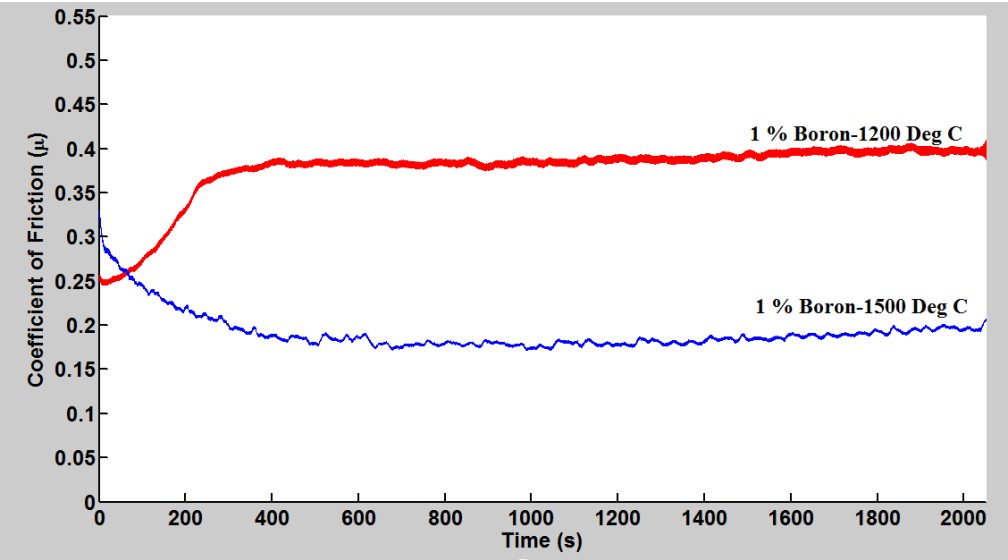

Figure 4.24. Coefficient of friction for 1 wt % boron composite sintered at 1200°C and 1500°C

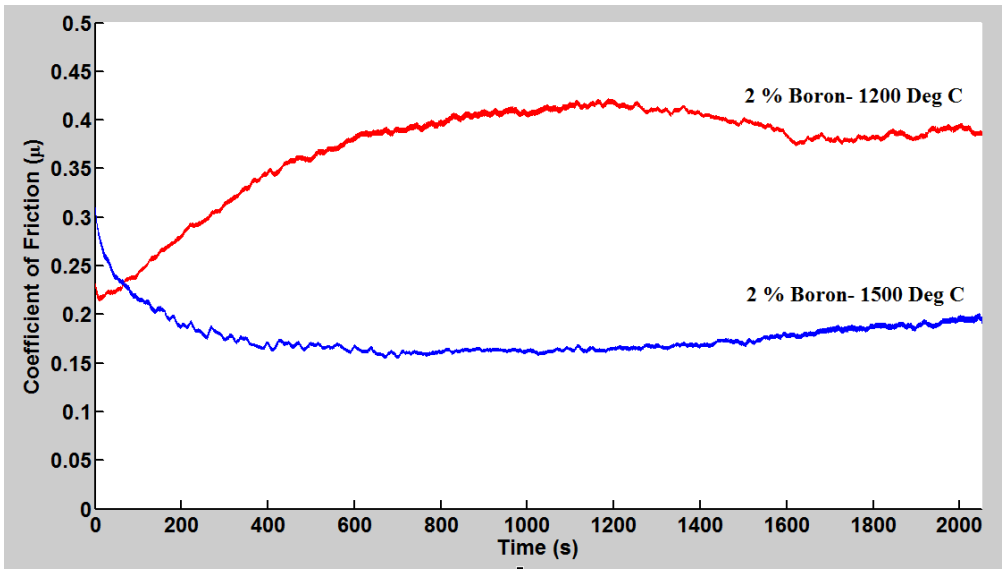

Figure 4.25. Coefficient of friction for 2 wt % boron composite sintered at 1200°C and 1500°C

Figure 4.26. shows the comparison of coefficient of friction for 3 wt % boron composite sintered at 1200°C and 1500°C. The behavior of this composite is similar to the above two composites. At the start of the test, the coefficient of friction was lower for the composites sintered at 1200°C (0.23). It gradually increased and stabilized at an average value of 0.54. For the composite sintered at 1500°C, the coefficient of friction initially started at a slightly higher value of 0.35. It gradually decreased with time and stabilized at a value of 0.32 by the end of the test period.

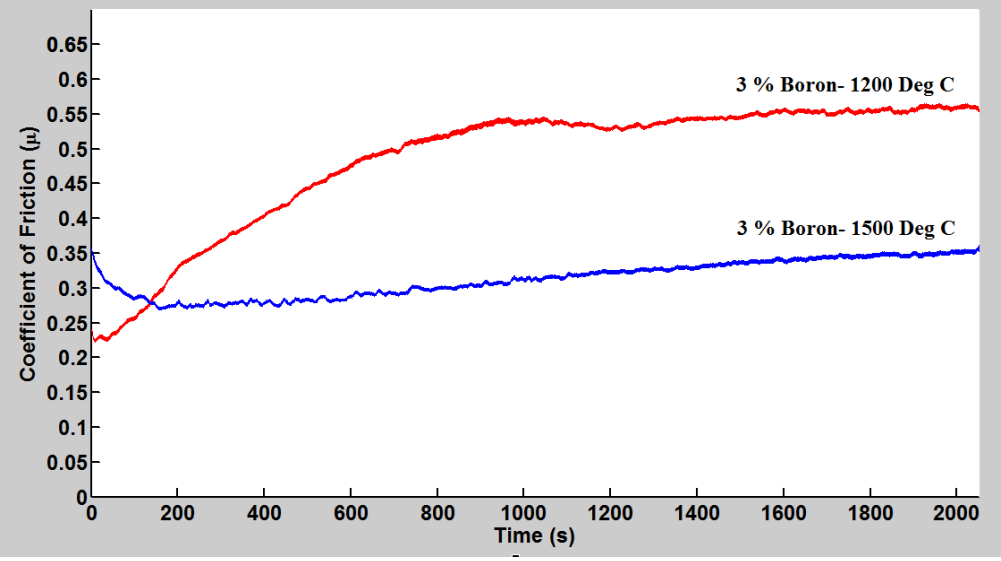

Figure 4.26. Coefficient of friction for 3 wt % boron composite sintered at 1200°C and 1500°C

General friction behavior of friction is the same for all the composites sintered at 1200°C and 1500°C. The coefficient of friction at the start of the test was higher for the

composites sintered at 1500°C and lower for composites sintered at 1200°C. It gradually increased and stabilized at the end of the test period for composites sintered at 1200°C. Coefficient of friction gradually decreased and stabilized for composites sintered at 1500°C.

4.3.1.1 Effect of Sintering Temperature and Concentration of Boron on Friction

As discussed in Section 4.1.1, orthorhombic $Al_{18}B_4O_{33}$ and hexagonal close-packed AlB_2 were found in the matrix for composites sintered at 1200°C. Properties of these phases are as shown in Table 4.1. AlB_2 has layered crystal structure which is similar to layered Molybdenum disulphide (MoS_2). The molybdenum atoms are in between the layers of sulphur atoms. Due to weak vander Waal forces between the layers of sulfide atoms, it has low shear strength which results in low coefficient of friction [99]. Similarly, aluminum atoms are loacted at the centers of hexagonal prisms which are formed by the boron sheets as shown in Figure 4.27.

The presence of this phase provided low friction in composites sintered at 1200°C. This friction is lower compared to pure alumina. For all the composites sintered at 1200°C with increase in wt % of boron, the coefficient of friction increased. This increase in hard $Al_{18}B_4O_{33}$ phases might have increased the coefficient of friction.

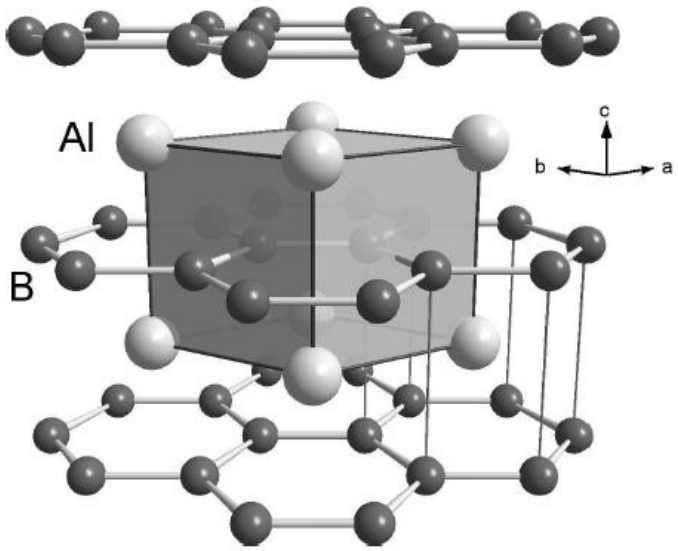

Figure 4.27. Schematic of layered crystal sturcture of AlB_2 [100]

Table 4.1. Properties of $Al_{18}B_4O_{33}$ and AlB_2

Material Properties	***AlB_2***	***$Al_{18}B_4O_{33}$***
Density (g/cc)	3.19 [101]	2.93 [102]
Melting point (^oC)	1655	1440
Young's modulus (GPa)	-	70-75 [103]
Hardness, (GPa)	15.0 [104]	11-15 [105]

XRD results showed the presence of AlB_2 and no dominating peaks of $Al_{18}B_4O_{33}$ for composites sintered at 1500^{o}C as discussed in Section 4.1.1. $Al_{18}B_4O_{33}$ is not stable at temperatures above 1400^{o}C. It decomposes into Al_2O_3 and B_2O_3 (g) at temperatures above 1400^{o}C. The following equation shows the decomposition of $Al_{18}B_4O_{33}$ [106].

$$\tfrac{1}{2}\,Al_{18}B_4O_{33} \xrightarrow{\text{Above } 1400^{o}C} 9/2\,Al_2O_3 + B_2O_3\,(g)\uparrow$$

As a result a new phase, B_2O_3 (g) formed which also has hexagonal crystal structure. The reduction in $Al_{18}B_4O_{33}$ phase and presence of B_2O_3 and AlB_2 might have resulted in further decrease of coefficient of friction. Within the composites sintered at 1500^{o}C with increase in wt % of boron, the coefficient of friction increased. The decomposition of $Al_{18}B_4O_{33}$ phase resulted in higher porosity. In the presence of pores, the nucleation of crack is more predominant due to the presence of high stress concentration areas. This results in enhanced cracking along the grain boundaries, which becomes more with increase in porosity. The microcracking or grain pullout results in generation of wear debris particles in the path of the wear track thereby increasing the contact area. This leads to increase in coefficient of friction [107].

For composites sintered at 1500^{o}C, the initial friction was high. But as the surface was worn, the B_2O_3 entrapped in the bulk was exposed to the surface which further reduced the friction. Figure 4.28 shows a schematic of porosity on the surface after decomposition of $Al_{18}B_4O_{33}$ phase. The gaseous B_2O_3 might have entrapped and condensed as liquid or solidified. This phase was shown in FTIR results.

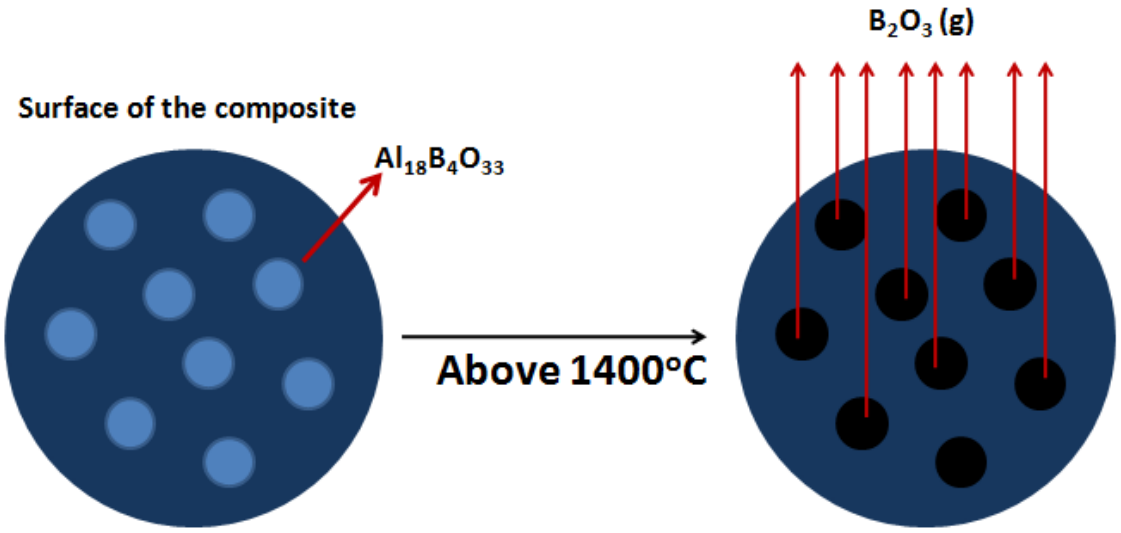

Figure 4.28. Schematic of surface porosity formed due to decomposition of $Al_{18}B_4O_{33}$

4.3.2 Wear Behavior

Figure 4.29 (a) shows the optical microscopic image of wear track for 3 wt % boron composite sintered at 1200°C. The central dark color track on the surface of the composite is the wear track formed due to sliding of steel ball. The steel ball was worn out. The transfer material was found on the wear track after the test. The worn surface of the steel ball is as shown in the Figure 4.29 (b).

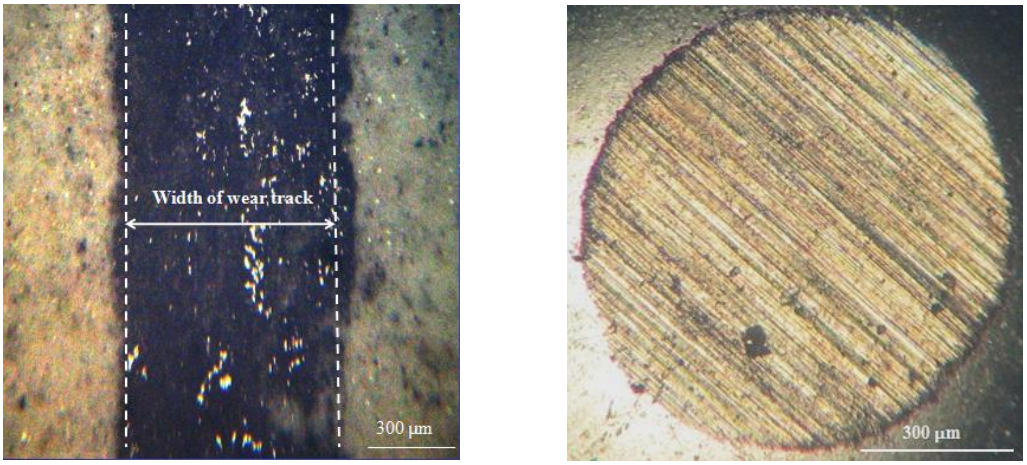

(a) (b)

Figure 4.29. Optical micrograph of (a) wear track (b) wear scar on steel surface for 2 wt % boron composite sintered at 1200^{o}C

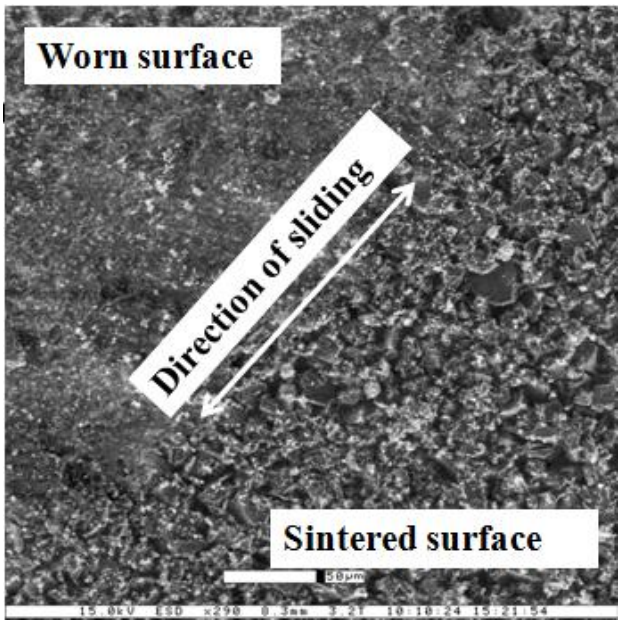

Figure 4.30. ESEM micrograph showing the wear track-sintered surface interface for 2 wt % boron composite sintered at 1200^{o}C

Figure 4.30 and Figure 4.31 show the interface of wear track and sintered surface. The wear track is comparatively smoother than the sintered surface. The difference between the composites before and after sliding for 1 wt % boron composite sintered at 1200^{o}C is shown in Figure 4.32. The smoother worn surfaces might be due to the smearing or smaller sized debris particles (0.5-3μm) filled in the pores.

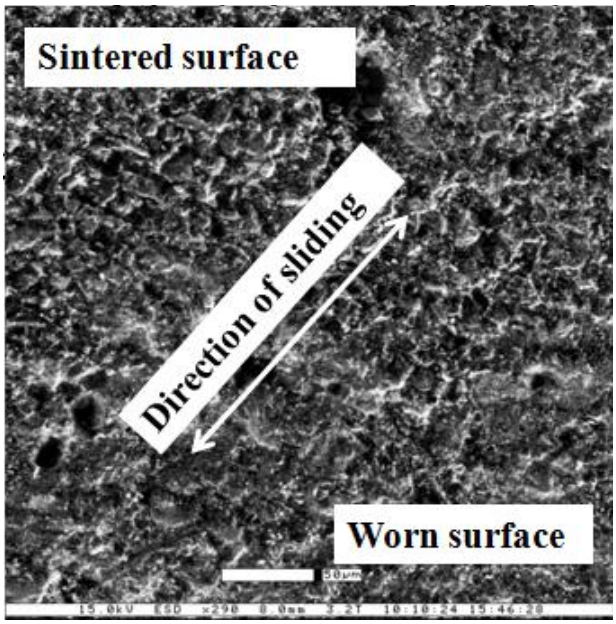

Figure 4.31. ESEM micrograph showing the wear track-sintered surface interface for 3 wt % boron composite sintered at 1200^{o}C

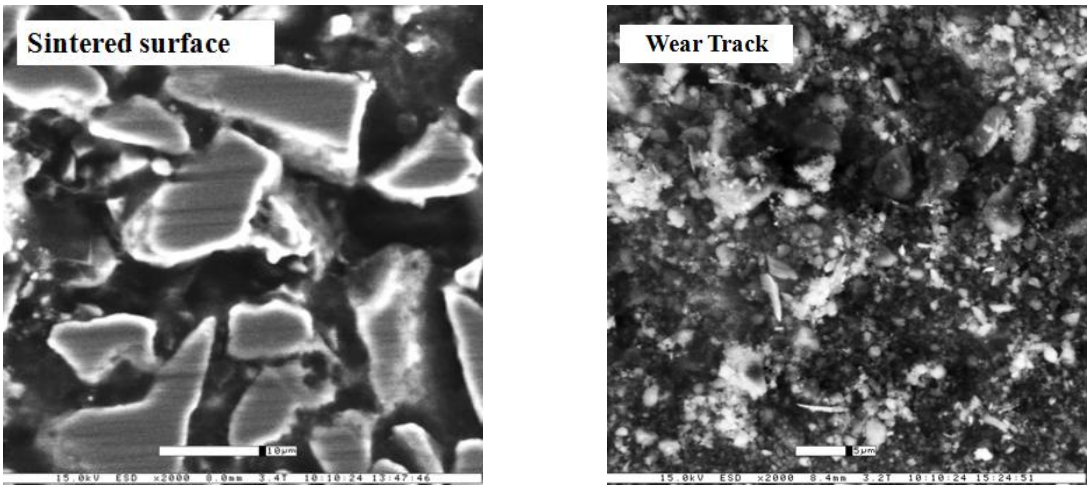

(a) (b)

Figure 4.32. ESEM micrographs showing (a) composite surface (b) worn surface for 1 wt % composite sintered at 1200^{o}C

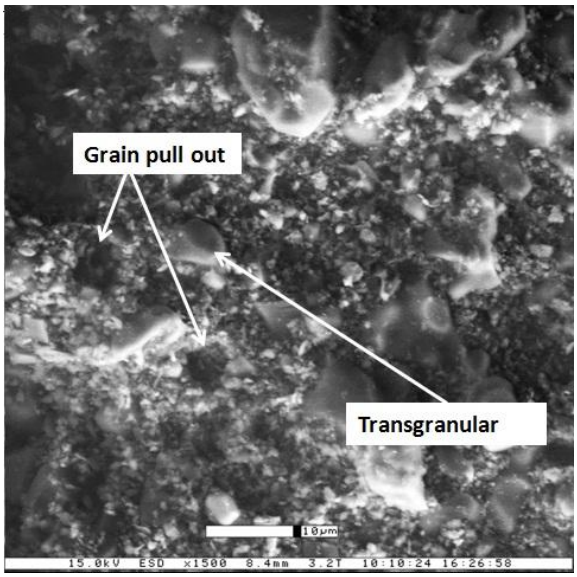

Figure 4.33. ESEM micrograph of wear track showing grain pullout and micro-cracks for composite sintered at 1200^{o}C

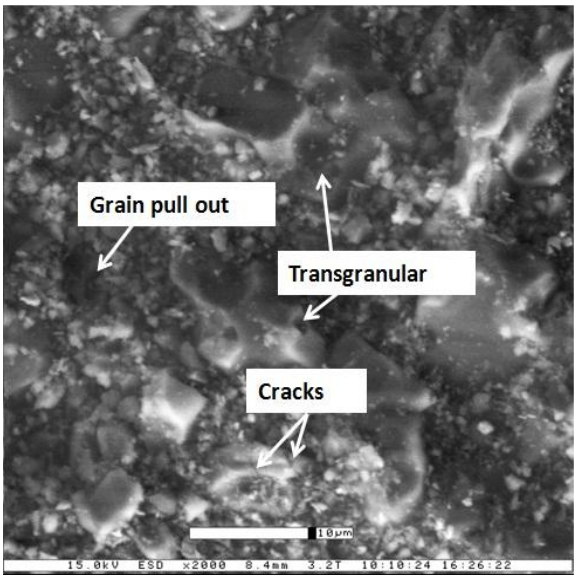

Figure 4.34. ESEM micrograph of wear track showing grain pullout and micro-cracks for composite sintered at 1500^{o}C

The size of the particles present on the worn surface is smaller due to fracture than those on the sintered surface. Evidence of micro-cracks was observed on the worn surface from Figure 4.33 and Figure 4.34. This indicates that grains failed due to brittle fracture. This is the transgranular mode of failure in which the path of failure is along the grains. There was also evidence of grain pullout. This shows intergranular failure in which the failure path is along the grain boundaries. This indicated that the composites failed in mixed mode i.e. both transgranular and intergranular mode.

4.3.3 Wear on the Sliding Counterface

During the sliding process between alumina composites and steel ball, wear was found on the both the interfaces. Wear volume was calculated for all the steel balls used for wear test using the formula

$$V = [(\pi r^4)/4R] \quad (12)$$

where 'R' is the radius of the counterpart, 'r' is the microscopic determination of the wear scar radius [108]. Figure 4.35 shows a schematic of wear scar radius measurement.

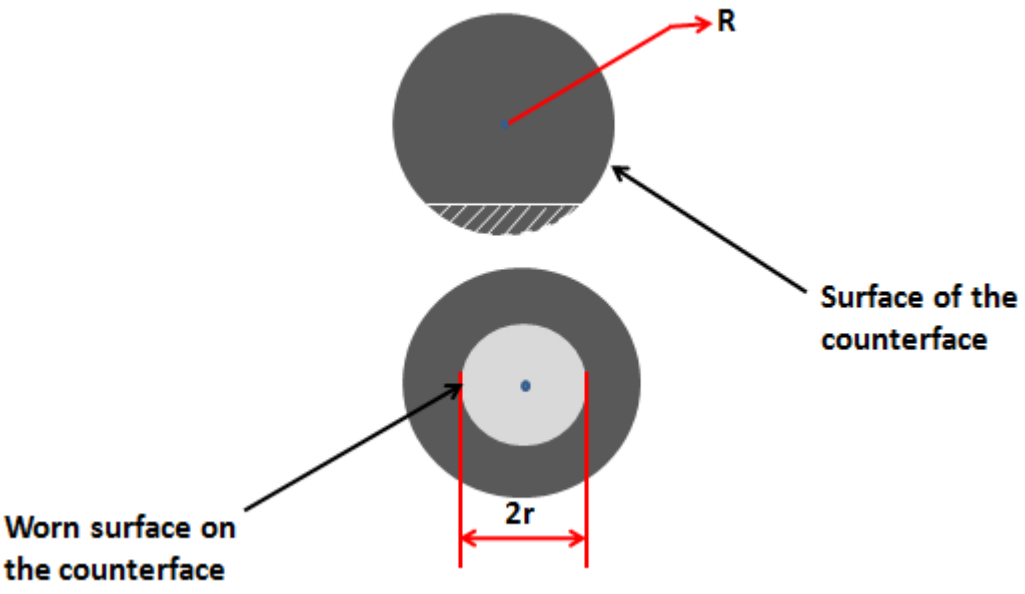

Figure 4.35. Schematic of wear scar measurement

Figure 4.29 (b) shows an optical micrograph of wear scar on steel ball after sliding. The calculated wear values are listed in the Table 4.2 for all the steel balls used.

Table 4.2. Wear volume of the steel ball at different sintering temperatures

Parameters	***1 % Boron***	***2 % Boron***	***3 % Boron***
1200^{o}C	14.23 x 10^{-12} m^3	4.01 x 10^{-12} m^3	2.016 x 10^{-12} m^3
1500^{o}C	3.62 x 10^{-12} m^3	2.575 x 10^{-12} m^3	4.42 x 10^{-12} m^3

The wear volume was comparatively lower for the steel balls used when slid against composites sintered at 1500^{o}C. The lowest wear volume was observed when slid against 3 wt % boron composite sintered at 1200^{o}C. The higher wear rate for the 3 wt % composite sintered at 1500^{o}C might be due to higher porosity.

Comparison of wear volume and coefficient of friction at all compositions for composites sintered at 1200^{o}C and 1500^{o}C respectively are shown in Figures 4.36 and Figure 4.37. The combination of composition and sintering temperature of a composite can be selected depending on the type of application. For example, for low friction and low wear, 1 wt % boron composite sintered at 1200^{o}C can be selected.

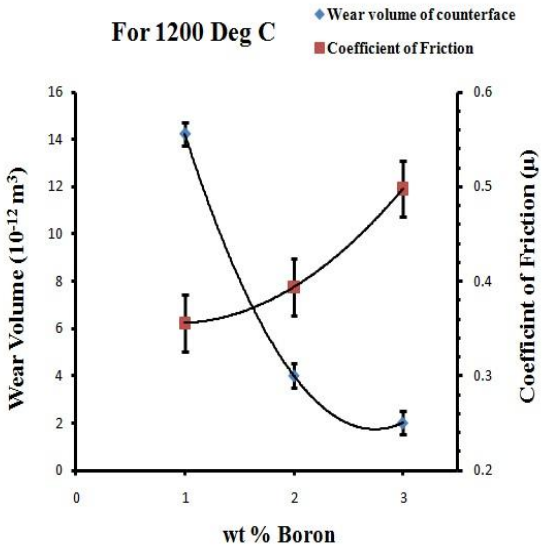

Figure 4.36. Comparison of wear volume and coefficient of friction for composites sintered at 1200°C

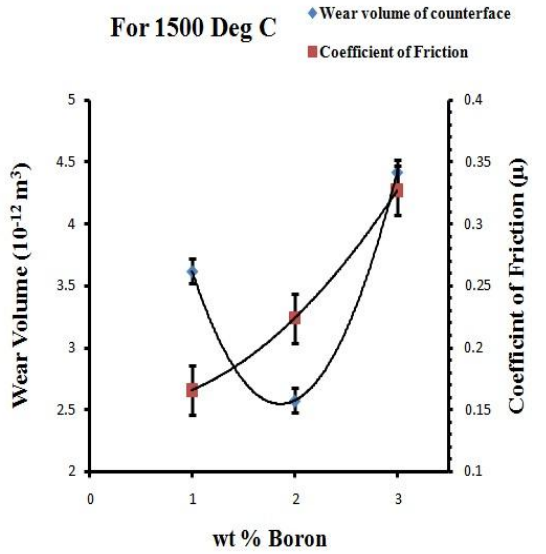

Figure 4.37. Comparison of wear volume and coefficient of friction for composites sintered at 1500°C

4.3.4 Wear Debris Analysis

Figure 4.38 and Figure 4.39 show the SE image and EDS spectra of 3 wt % composite sintered at 1200^{o}C respectively. It is evident from Figure 4.38 that the wear debris particles are smaller in size compared to the size of grains in the composite (Figure 4.11 (b)). The size of the debris particles is ~ 0.5-3μm.

The EDS results show that significant amounts of aluminum, carbon, boron, oxygen, silicon, iron, and chromium are present on the wear track. This indicates that the transfer of material from the AISI steel counterface to the composite surface has taken place. The chemical composition of the steel counterface is shown in Table 4.3.

Table 4.3. Chemical composition of AISI 52100 bearing ball [109]

Elements	***Composition***
Carbon (C)	0.980 - 1.10 %
Chromium (Cr)	1.30 - 1.60 %
Iron (Fe)	96.5 - 97.32 %
Manganese (Mn)	0.250 - 0.450 %
Phosphorous (P)	<= 0.0250 %
Silicon (Si)	0.150 - 0.300 %
Sulphur (S)	<= 0.0250 %

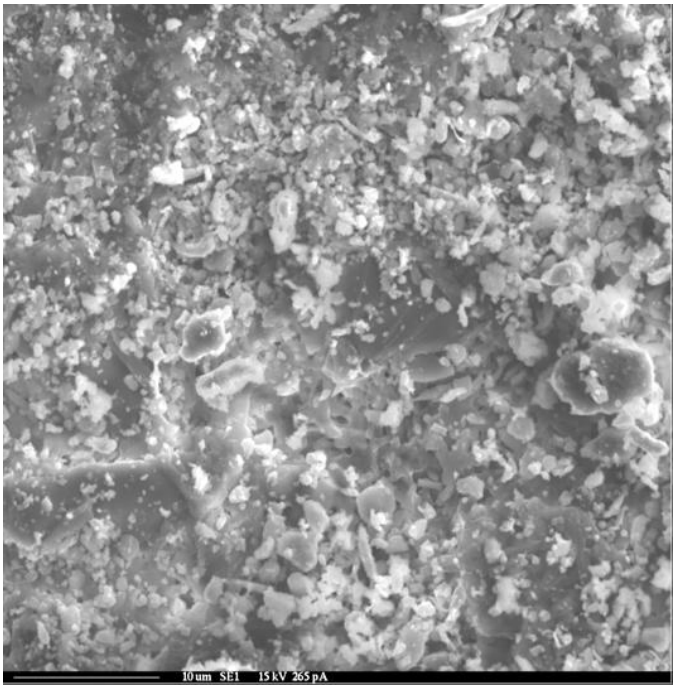

Figure 4.38. SE image of wear track for 3 wt % composite sintered at 1200°C

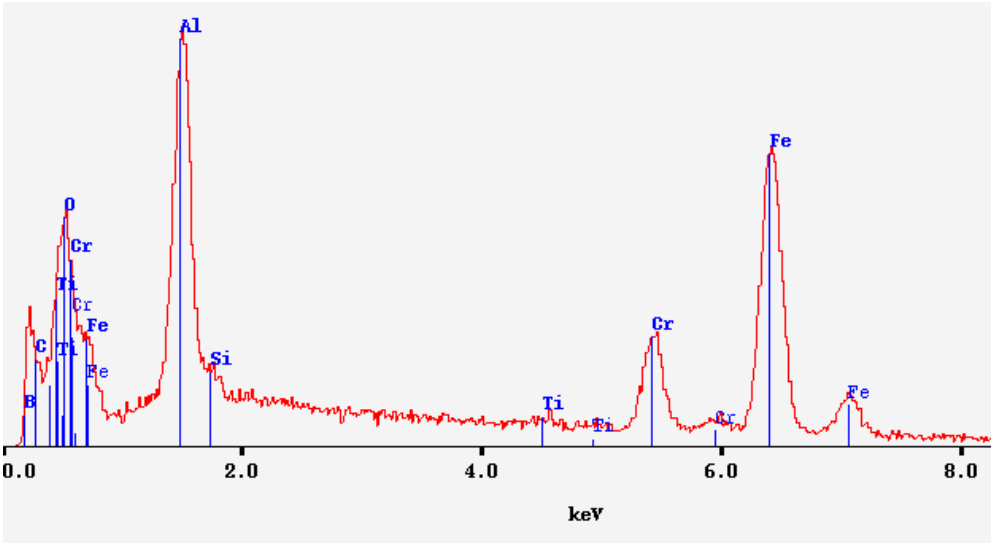

Figure 4.39. EDS spectrum of debris for 3 wt % composite sintered at 1200°C

CHAPTER V

CONCLUSIONS AND FUTURE RECOMMENDATIONS*

This thesis studied the synthesis and tribological characterization of novel alumina based ceramic composites for low friction applications. Investigations have been conducted on two areas. Firstly, the effect of sintering temperature and wt % of boron on physical and mechanical properties of the composites has been investigated. Secondly, the effect of sintering temperature and wt % of boron on surface and tribological properties of the composites has been studied. The results obtained from these investigations led to the following conclusions and recommendations for future studies.

5.1. Physical and Mechanical Characterization

XRD results confirmed the formation of $Al_{18}B_4O_{33}$, and AlB_2 and FTIR confirmed the presence of B_2O_3. The formation of $Al_{18}B_4O_{33}$ reduced with increase in sintering temperature and wt% of boron. Increase in sintering temperature and wt % of boron affected the porosity, grain size, and hardness of the composites. The absence of $Al_{18}B_4O_{33}$ phase at 1500^oC reduced the density of the composites compared to composites sintered at 1200^oC.

---

* Reprinted with permission from Paluri, R., Ingole, S.: Surface characterization of novel alumina-based composites for energy efficient sliding systems. Journal of Materials. **63**, 77-83 (2011), Copyright [2011] by The Minerals, Metals & Materials Society.

Porosity was higher for the composites sintered at 1500^{o}C. Grain size decreased with increase in sintering temperature and wt % of boron due to presence of secondary phases at the grain boundaries. The composites sintered at 1200^{o}C were harder than those sintered at 1500^{o}C due to the presence of harder $Al_{18}B_4O_{33}$ phase and higher porosity.

5.2. Surface and Tribological Characterization

The decomposition of the $Al_{18}B_4O_{33}$ phase changed the texture of the composites. The composites sintered at 1500^{o}C have higher surface roughness compared to composites sintered at 1200^{o}C due to higher surface porosity.

The coefficient of friction was lower for the composites compared to pure alumina ceramic. The coefficient of friction decreased with increase in sintering temperature. The decomposition of $Al_{18}B_4O_{33}$ phase and presence of AlB_2 and B_2O_3 phases provided lower friction for composites sintered at 1500^{o}C. The wear mechanism was found to be micro-fracture using ESEM and SEM studies. The wear volume of the steel counterface when slid against the composites was also very low compared to pure alumina. Thus, composites with optimum coefficient of friction and wear volume of the counterface can be selected depending on the application.

5.3. Future Recommendations

1. Study the friction and wear behavior of the composites using alumina as counterface.

2. Study the effect of testing parameters i.e., load, temperature, etc on friction and wear behavior of the composites.

REFERENCES

[1] Bhushan, B.: Introduction to tribology, John Wiley and Sons, New York (2002)

[2] Jost, H. P.: Tribology: How a word was coined 40 years ago. Journal of Friction and Wear. **27**, 1-3 (2006)

[3] Ko, Y. M., Kwon, W. T., Kim, Y. W.: Development of Al_2O_3–SiC composite tool for machining application. Ceramics International. **30**, 2081-2086 (2004)

[4] Mang, T., Dresel, W.: Lubricants and lubrication, Wiley-VCH, Weinheim, Germany (2007)

[5] Elvik, R., Hoye, A., Vaa, T., Sorensen, M.: The handbook of road safety measures, Emerald Group Publishing, Bingley, UK (2009)

[6] Carmody, S., Website: http://machinedesign.com/article/high-friction-coating-puts-the-brakes-on-descent-to-mars-1211, last accessed in December (2010)

[7] Biswas, S. K., Vijayan, K.: Friction and wear of PTFE – A review. Wear. **158**, 193-211 (1992)

[8] Donnet, C., Martin, J. M., LeMogne, T., Belin, M.: Super-low friction of MoS_2 coatings in various environments. Tribology International. **29**, 123-128 (1996)

[9] Zhang, S. Y., Zhu, W. G.: Tin coating of tool steels - A review. Journal of Materials Processing Technology. **39**, 165-177 (1993)

[10] Ahrens, C. D.: Meteorology today: An introduction to weather, climate, and the environment, Thomson/Brooks/Cole, Pacific Grove, CA (2007)

[11] Kjaer, C., Douglas, B., Bianchin, R., Zander, E.: Wind energy-- the facts: A guide to the technology, economics and future of wind power, Earthscan, London, UK (2009)

[12] Basavakumar, K. G., Mukunda, P. G., Chakraborty, M.: Influence of melt treatments on sliding wear behavior of Al-7Si and Al-7Si-2.5Cu cast alloys. Journal of Materials Science. **42**, 7882-7893 (2007)

[13] Blau, P. J.: Friction science and technology: From concepts to applications, CRC Press, New York (2009)

[14] Rabinowicz, E.: Tribology and mechanics of magnetic storage systems, ASME, New York (1986)

[15] Rabinowicz, E.: Friction and wear of materials, John Wiley & Sons, New York (1995)

[16] Jost, H. P.: Tribology- origin and future. Wear. **136**, 1-17 (1990)

[17] Barsoum, M. W.: Fundamentals of ceramics, Francis and Taylor, New York (2002)

[18] Davis, J. R., Editor: ASM specialty handbook, tool materials. ASM International, Materials Park, OH (1995)

[19] Baldus, P., Jansen, M., Sporn, D.: Ceramic fibers for matrix composites in high-temperature engine applications. Science. **285**, 699-703 (1999)

[20] Morrell, R.: Handbook of properties of technical ceramics. Part 1. An introduction for the engineer and designer, Her Majesty's Stationery Office, Great Britan, UK (1987)

[21] Chenje, T. W.: Relationship between microstructure, hardness, impact toughness and wear performance of selected grinding media for mineral ore milling operations. Materials and Design. **25**, 11-18 (2004)

[22] Wiederhorn, S. M.: Brittle fracture and toughening mechanisms in ceramics. Annual Review of Materials Science. **14**, 373-403 (1984)

[23] Hasselman, D.P.H, Fulrath, R. M.: Proposed fracture theory of a dispersion-strengthened glass matrix. Journal of the American Ceramic Society. **49**, 68-72 (1966)

[24] Green, D. J.: Fracture toughness predictions for crack bowing in brittle particulate composites. Journal of the American Ceramic Society. **66**, C-4-C-5 (1983)

[25] Rong, S., Ji, Z., Zhu, Y., Zhang, J.: Effect of rod-like grain on properties and toughening mechanism of 3Y-TZP/Al_2O_3 ceramics. Transactions of Nonferrous Metals Society of China. **18**, 388-392 (2008)

[26] Evans, A. G., Faber, K. T.: Toughening of ceramics by circumferential microcracking. Journal of the American Ceramic Society. **64**, 394-398 (1981)

[27] Xie, Z., Gao, L., Li, W., Xu, L., Wang, X.: High toughness alumina ceramics with elongated grains developed from seeds. Science in China Series E: Technological Sciences. **46**, 527-536 (2003)

[28] Porter, D. L., Heuer, A. H.: Mechanisms of toughening partially stabilized zirconia (PSZ). Journal of the American Ceramic Society. **60**, 183-184 (1977)

[29] Webb, W. W.: Dislocation structure and the formation and strength of sodium chloride whiskers. Journal of Applied Physics. **31**, 194-206 (1960)

[30] Rödel, J., Fuller, E. R., Lawn, B. R.: In situ observations of toughening processes in alumina reinforced with silicon carbide whiskers. Journal of the American Ceramic Society. **74**, 3154-3157 (1991)

[31] Tani, T., Miyamotoa, Y., Koizumia, M., Shimada, M.: Grain size dependences of Vickers microhardness and fracture previous toughness in Al_2O_3 and Y_2O_3 ceramics. Ceramics International. **12**, 33-37 (1986)

[32] Muchtar, A., Lim, L. C.: Indentation fracture toughness of high purity submicron alumina. Acta Metallurgica. **46**, 1683-1698 (1998)

[33] Mishra, R. S., Mukherjee, A. K.: Processing of high hardness-high toughness alumina matrix nanocomposites. Material Science and Engineering. **A301**, 97-101 (2001)

[34] Esposito, L., Tucci, A.: Microstructural dependence of friction and wear behaviors in low purity alumina ceramics. Wear. **205**, 88-96 (1997)

[35] Naglieri, V., Joly-Pottuz, L., Chevalier, J., Lombardi, M., Montanaro, L.: Follow-up of zirconia crystallization on a surface modified alumina powder. Journal of the European Ceramic Society. **30**, 3377-3387 (2010)

[36] Lee, W., Rainforth, W. M.: Ceramic microstructures: Property control by processing, Chapman and Hall, London, UK (1994)

[37] Louet, N., Reveron, H., Fantozzi, G.: Sintering behaviour and microstructural evolution of ultrapure α-alumina containing low amounts of SiO_2. Journal of the European Ceramic Society. **28**, 205-215 (2007)

[38] Liu, J., Ownby, D.: Boron containing ceramic particulate and whisker enhancement of the fracture toughness of ceramic matrix composites. AIP Conference Proceedings. **231**, 574-577 (1991)

[39] Nivot, C., Valdivieso, F., Goeuriot, P.: Nitrogen pressure effects on non-isothermal alumina sintering. Journal of the European Ceramic Society. **26**, 9-15 (2006)

[40] Kim, I.-S., Lee, S.-J.: Effects of alumina type and attritor ball size on the processing of RBAO – ZrO_2 ceramics. Materials Letters. **48**, 247-251 (2001)

[41] Wang, H. Z., Gao, L., Gui, L. H., Guo, J. K.: Preparation and properties of intragranular Al_2O_3-SiC nanocomposites. Nanostructured Materials. **10**, 947-953 (1998)

[42] Totten, G. E., MacKenzie, D. S.: Handbook of aluminum: Physical metallurgy and processes, Marcel Dekker, Inc., New York (2003)

[43] The American Ceramic Society, Phase diagrams for ceramists, The American Ceramic Society, Columbus, OH (1975)

[44] Wang, J., Stevens, R.: Review zirconia-toughened alumina (ZTA) ceramics. Journal of Materials Science. **24**, 3421-3440 (1989)

[45] Huang, C., Wang, J.: Sintering behavior and microwave dielectric properties of nano alpha-alumina. Materials Letters. **59**, 3746-3749 (2005)

[46] Karihaloo, B.: Contribution of t → m phase transformation to the toughening of ZTA. Journal of American Ceramics Society. **74**, 1703-1706 (1991)

[47] Hori, S., Yoshimura, M., Somiya, S.: Strength-toughness relations in sintered and isostatically hot-pressed ZrO_2-toughened Al_2O_3. Journal of American Ceramics Society. **69**, 169-172 (1986)

[48] Becher, P. F., Alexander, K. B., Warmick, W.: Influence of ZrO_2 grain size and content on the transformation response in the Al_2O_3-ZrO_2 (12 mol% CeO_2) System. Journal of American Ceramics Society. **76**, 657-663 (1993)

[49] Casellas, D., Nagl, M. M., Llanes, L., Anglada, M.: Fracture toughness of Alumina and ZTA ceramics: microstructural coarsening effects. In: International Conference on the Advanced Materials Processing Technology, 148-152, (2001)

[50] Heuer, A. H., Lange, F. F., Swain, M. V., Evans, A. G.: Transformation toughening: An overview. Journal of the American Ceramic Society. **69**, i-iv (1986)

[51] Cai, K. F., McLachlan, D. S., Axen, N., Manyatsa, R.: Preparation, microstructures and properties of Al_2O_3 –TiC composites. Ceramics International. **28**, 217-222 (2002)

[52] You, X. Q., Si, T. Z., Liu, N., Ren, P. P., Xu, Y.D., Feng, J. P.: Effect of grain size on thermal shock resistance of Al_2O_3–TiC ceramics. Ceramics International. **31**, 33-38 (2005)

[53] Wang, L., Shi, J. L., Hua, Z.-L.: The influence of addition of WC particles on mechanical properties of alumina–matrix composite. Materials Letters. **50**, 179-182 (2000)

[54] Sternitzke, M., Derby, B., Brook, R. J.: Alumina/silicon carbide nanocomposites by hybrid polymer/powder processing: microstructures and mechanical properties. Journal of American Ceramics Society. **81**, 41-48 (1998)

[55] Ko, Y. M., Kwon, W. T., Kim, Y. W.: Development of Al_2O_3–SiC composite tool for machining application. Ceramics International. **30**, 2081-2086 (2004)

[56] Niihara, K.: New design concept of structural ceramics-ceramic nanocomposites. Journal of Ceramics Society of Japan. **99**, 974-982 (1991)

[57] Nakao, W., Mori, S., Nakamura, J., Takahashi, K., Ando, K., Yokouchi, M.: Self-crack-healing behavior of mullite/SiC particle/SiC whisker multi-composite and potential use for ceramic springs. Journal of American Ceramics Society. **89**, 1352-1357 (2005)

[58] Lackey, W. J., Stinton, D. P., Cermy, G. A., Schaffhauser, A. C., Fehrenbacher, L. L.: Ceramic coatings for advanced heat engines—A review and projection. Advanced Ceramic Materials. **2**, 24-30 (1987)

[59] Liu, J., Ownby, D.: Boron carbide reinforced alumina composites. Journal of American Ceramics Society. **74**, 674-677 (1991)

[60] Benko, E., Morgiel, J., Czeppe, T.: BN sintered with Al: microstructure and hardness. Ceramics International. **23**, 89-94 (1997)

[61] Ohash, T., Yamamoto, K., Hamada, Y., Tanase, T.: Some properties and cutting performance of polycrystalline cubic boron nitride with no additives. International Journal of Refractory Metals and Hard Materials. **16**, 403-407 (1998)

[62] Shonhiwa, A., Herrmann, M., Sigalas, I., Coville, N.: Reaction bonded aluminum oxide composites containing cubic boron nitride. Ceramics International. **35**, 909-911 (2009)

[63] Bhushan, B.: Principles and applications of tribology, Wiley-IEEE, New York (1999)

[64] Takadoum, J.: Materials and surface engineering in tribology, John Wiley and Sons, New York (2008)

[65] Bhushan, B.: Fundamentals of tribology and bridging the gap between the macro- and micro/nanoscales, Kluwer Academic Publishers, Norwell, MA (2001)

[66] Geike, T., Popov, V. L.: Multi-layer models of friction between solids. Tribology International. **39**, 437-443 (2006)

[67] Bowden, F. P., Tabor, D.: The friction and lubrication of solid, Oxford, Clarendon, UK (1964)

[68] Rohatgi, P. K., Ray, S., Liu, Y.: Tribological properties of metal matrix-graphite particle composites International Materials Reviews. **37**, 129-152 (1992)

[69] Singer, I. L.: Mechanics and chemistry of solids in sliding contact. Langmuir. **12**, 4486-4491 (1996)

[70] Bridgeman, P. W.: Shearing phenomena at high pressure particularly in inorganic compounds. In: American Academy of Arts and Sciences, p. 387, (1936)

[71] Singer, I. L., Bolster, R. N., Wegand, J., Fayeulle, S., Stupp, B. C.: Hertzian stress contribution to low friction behavior of thin MoS_2 coatings. Applied Physics Letters. **57**, 995-997 (1990)

[72] Blau, P., Blau, P. J., Bayer, R. G.: Wear of materials: Proceedings of the Fourteenth International Conference on Wear of Materials, Elsevier, Washington, DC (2003)

[73] Narayan, R.: Biomedical materials, Springer, New York (2009)

[74] Khrushchov, M. M., Babichev, M. A.: Abrasive wear, Defense Technical Information Center, Fort Belvoir, VA (1971)

[75] Suh, N. P.: Tribophysics, Prentice Hall, Upper Saddle River, NJ (1986)

[76] Pearsall, K. J., Eliezer, Z., Amateau, M. F.: The effect of sliding time and speed on the wear of composite materials. Wear. **63**, 121-130 (1980)

[77] Sinanoglu, C., Nair, F., Karamis, M. B.: Effects of shaft surface texture on journal bearing pressure distribution. Journal of Materials Processing Technology. **168**, 344-353 (2005)

[78] Etsion, I.: Improving tribological performance of mechanical components by laser surface texturing. Tribology Letters. **17**, 733-737 (2004)

[79] Bhushan, B., Liu, H.: Nanotribological properties and mechanisms of alkylthiol and biphenyl thiol self-assembled monolayers studied by AFM. Physical Review B. **63**, p. 245412 (2001)

[80] Salehi, A., Tsai, S., Pawar, V., Sprague, J., Hunter, G., Varma, S. K., Namavar, F.: Wettability analysis of orthopaedic materials using optical contact angle methods. Key Engineering Materials. **390-311**, 1199-1202 (2006)

[81] Cassie, A. B. D., Baxter, S.: Wettability of porous surfaces. Transactions of the Faraday Society. **40**, 546-551 (1944)

[82] Jianxin, D., Tongkun, C., Zeliang, D., Jianhua, L., Junlong, S., Jinlong, Z.: Tribological behaviors of hot-pressed Al_2O_3/TiC ceramic composites with the additions of CaF_2 solid lubricants. Journal of the European Ceramic Society. **26**, 1317-1323 (2006)

[83] Gangopadhyay, A., Jahanmir, S.: Friction and wear characteristics of silicon nitride-graphite and alumina-graphite composites. Tribology Transactions. **34**, 257-265 (1991)

[84] Carrapichano, J. M., Gomes, J. R., Silva, R. F.: Tribological behaviour of Si_3N_4-BN ceramic materials for dry sliding applications. Wear. **253**, 1070-1076 (2002)

[85] Yu, L. Z., Ran, G. H., Xi, Z. M., Qin, H. X.: Preparation of aluminum borate whisker reinforced aluminum phosphate wave-transparent materials. Chinese Science Bulletin. **53**, 3073-3076 (2008)

[86] Owate, I., Freer, R.: Thermochemical etching method for ceramics. Journal of American Ceramics Society. **75**, 1266-1268 (1992)

[87] Horálek, V.: ASTM grain-size model and related random tessellation models. Materials Characterization. **25**, 263-284 (1990)

[88] Callister, W. D.: Materials science and engineering: An introduction. John Wiley & Sons, Inc, New York (2007)

[89] Nagendra, N., Bandopadhyay, S.: Strength and fracture toughness of LSFCO membranes exposed to reducing conditions. Scripta Materialia. **48**, 37-42 (2003)

[90] Barbato, G., Desogus, S.: Problems in the measurement of Vickers and Brinell indentations. Measurement. **4**, 137-147 (1986)

[91] Zhang, G. J., Yang, J. F., Ando, M., Ohji, T., Kanzaki, S.: Reactive synthesis of alumina-boron nitride composites. Acta Materialia. **52**, 1823–1835 (2004)

[92] Okamoto, H.: Al−B (aluminum-boron). Journal of Phase Equilibria and Diffusion. **27**, 195-196 (2006)

[93] Smith, B. C.: Fundamentals of Fourier transform infrared spectroscopy, CRC Press, New York (1996)

[94] Villegas, M., Sierra, T., Caballero, A. C., Fernandez, J. F.: Ti-based nanocoatings on Al_2O_3 powders. Ceramics International. **33**, 875-878 (2007)

[95] Oki, A., Adams, L., Luo, Z.: Solvothermal synthesis of carbon nanotube-B_2O_3 nanocomposite using tributyl borate as boron oxide source. Inorganic Chemistry Communications. **11**, 275-278 (2008)

[96] Wu, X., Wang, Z., Chen, L., Huang, X.: Carbon/B_2O_3 composite with higher capacity for lithium storage. Solid State Ionics. **170**, 117-121 (2004)

[97] Park, C. I., Jeong, H. E., Lee, S. H., Cho, H. S., Suh, K. Y.: Wetting transition and optimal design for microstructured surfaces with hydrophobic and hydrophilic materials. Journal of Colloid and Interface Science. **336**, 298-303 (2009)

[98] Pasaribu, H. R., Sloetjes, J. W., Schipper, D. J.: Friction reduction by adding copper oxide into alumina and zirconia ceramics. Wear. **255**, 699-707 (2003)

[99] Park, K. T., Richards-Babb, M., Freund, M. S., Weiss, J., Klier, K.: Surface structure of single-crystal MoS_2(0002) and Cs/MoS_2(0002) by X-ray photoelectron diffraction. The Journal of Physical Chemistry. **100**, 10739-10745 (1996)

[100] Loa, I., Kunc, K., Syassen, K., Bouvier, P.: Crystal structure and lattice dynamics of AlB_2 under pressure and implications for MgB_2. Physical Review B. **66**, 134101 (2002)

[101] Ulrich, B., Vladimir, G., Frank, H., Horst, B., Walter, S., Alexander, Y., Yuri, G.: On the electronic and structural properties of aluminum diboride $Al_{0.9}B_2$. Journal of Solid State Chemistry. **177**, 389-394 (2004)

[102] Peng, L. M., Li, X. K., Li, H., Wang, J. H., Gong, M.: Synthesis and microstructural characterization of aluminum borate whiskers. Ceramics International. **32**, 365-368 (2006)

[103] Zheng, M., Wu, K., Liang, H., Kamado, S., Kojima, Y.: Microstructure and mechanical properties of aluminum borate whisker-reinforced magnesium matrix composites. Materials Letters. **57**, 558-564 (2002)

[104] Kharlamov, A. I., Kirillova, N. V., Zaitseva, Z. A.: Properties of very fine aluminum boride and borocarbide powders and also hot-pressed materials based on them. Materials Letters. **34**, 229-238 (1995)

[105] Ray, S. P.: Preparation and characterization of aluminum borate. Journal of American Ceramics Society. **75**, 2505-2609 (1992)

[106] Blackburn, P. E., Büchler, A., Stauffer, J. L.: Thermodynamics of vaporization in the aluminum oxide—boron oxide system. The Journal of Physical Chemistry. **70**, 2469-2474 (1966)

[107] He, Y., Winnubst, L., Burggraaf, A. J., Verweij, H., Van der Varst, P. G. T., deWith, B.: Influence of porosity on friction and wear of tetragonal Zirconia polycrystal. Journal of the American Ceramic Society. **80**, 377-380 (1997)

[108] Erdemir, A., Fenske, G. R.: Tribological performance of diamond and diamond-like carbon films at elevated temperatures. Tribology Transactions. **39**, 787 - 794 (1996)

[109] ASM International: Properties and selection: Irons, steels, and high-performance alloys, Vol. 1, ASM International, Metals Park, OH (1990)

VITA

Name:	Rajeshwari S Lakshmi Paluri
Address:	C/O Dr. Hong Liang, Mechanical Engineering, Texas A&M University, College Station, Texas 77843-3123
Email Address:	rajeshwaripsl@gmail.com
Education:	B.E., Mechanical Engineering, Osmania University, 2008 M.S., Mechanical Engineering, Texas A&M University, 2011
Research Interests:	Tribology, Ceramics, Coatings